row, spleen, thymus, and lymph nodes; in the gastrointestinal tract from the tongue to the rectum; in reproductive organs including testis, epididymis, seminal vesicle, prostate gland, ovary, and uterus; or in the epidermis and dermis of the skin (unpublished data). In addition, no marked difference in systolic blood pressure, as measured by a noninvasive tail-cuff method, was found between wild-type and ROCK-I$^{-/-}$ mice (138 ± 10 and 134 ± 6 mmHg, respectively, $n = 5$).

Impaired extension of the eyelid epithelial sheet in ROCK-I$^{-/-}$ embryos

To elucidate the molecular mechanism responsible for the failure of eyelid closure in ROCK-I$^{-/-}$ embryos, we first examined wild-type and homozygous mutant embryos at various stages by scanning electron microscopy (Fig. 3 A). Typically, at 14.5 dpc, wild-type and ROCK-I$^{-/-}$ embryos manifested open eyes of similar shape and with no distinct morphological difference. Differences between the genotypes were evident at 15.5 and 16.0 dpc, however. In wild-type embryos, the rims of the top and bottom eyelids extended toward each other and fused from both nasal and lateral margins. In contrast, the eyelids of many ROCK-I$^{-/-}$ embryos failed to extend during this period, leaving the ocular surface exposed. Whereas the eyelids of wild-type embryos were completely fused at the midline by 16.5 dpc, two different degrees of failure of eyelid closure (fully open eyes or partially fused eyelids) were apparent in the eyes of ROCK-I$^{-/-}$ mice at this time.

We next compared eyelid closure in wild-type and ROCK-I$^{-/-}$ embryos by histological analysis (Fig. 3 B). Similar to the skin in other regions of the body, the eyelid consists of epithelium and dermis. In wild-type embryos, the eyelid epithelium comprises a single layer of basal cells at 14.5 dpc and becomes multilayered as a result of proliferation and differentiation of the basal cells between 15.5 and 16.0 dpc. Around this time, the eyelid epithelial sheet extends from both top and bottom eyelid tips to cover the ocular surface. The two sheets meet at the center and eventually fuse each other at 16.5 dpc. The eyelid morphology of ROCK-I$^{-/-}$ embryos appeared identical to that of their wild-type littermates at 14.5 dpc. The eyelid epithelium also became multilayered in the mutant mice between 15.5 and 16.0 dpc. However, the ROCK-I$^{-/-}$ embryos failed to extend the eyelid epithelial sheet. At 16.5 dpc, the ROCK-I$^{-/-}$ embryos had only partially extended the eyelid epithelial sheets or had not done so at all. Consequently, the eye of ROCK-I$^{-/-}$ embryos was open by varying degrees at 18.5 dpc. These results suggest that the EOB phenotype of ROCK-I$^{-/-}$ mice is caused by impaired or delayed extension of the eyelid epithelial sheet.

To characterize the cells present in the eyelid epithelial sheet, we performed immunofluorescence staining for keratins 5, 10, and 6, which are markers of epithelial cell differentiation (Fig. 3 C; Fuchs, 1996; Mazzalupo and Coulombe, 2001). The eyelid epithelial sheet of wild-type embryos was positive for keratin 5 and negative for keratin 10, indicative of its basal cell composition. The sheet was also positive for keratin 6. A similar staining pattern was apparent for the cell mass at the expected site of sheet formation in ROCK-I$^{-/-}$ mice. In addition, the base of the eyelid epithelial sheet in wild-type embryos and that of the cell mass in ROCK-I$^{-/-}$ embryos were rich in cells positive for Ki67, a marker of cell proliferation. These results indicate the presence of a population of normally differentiated cells in the eyelid of ROCK-I$^{-/-}$ mice.

Impaired formation of actomyosin cables in the eyelid epithelial cells of ROCK-I$^{-/-}$ embryos

Given that ROCK induces myosin-mediated cross-linking of actin filaments and consequently makes actin bundles such as stress fibers in cultured cells, we investigated whether loss of ROCK-I might impair formation of the actin architecture required for extension of the eyelid epithelial sheet and thereby cause the EOB phenotype. Whole-mount phalloidin staining of the eyelids of wild-type embryos at 15.5 and 16.0 dpc revealed the presence of thick actin cables that coursed continuously from cell to cell at the leading edge of the eyelid epithelial sheet and encompassed the circumference of the eye like a ring (Fig. 4, A–D). Pronounced phalloidin staining was also apparent in individual cells of the eyelid around the eye circumference in ROCK-I$^{-/-}$ embryos, but most of these actin filaments were not organized into cables that extended beyond each cell (Fig. 4, A and E–G). Phalloidin staining of transverse frozen sections from wild-type mice revealed that the actin cables were localized in a few layers of cells in the eyelid epithelial sheet (Fig. 4 H); they were first apparent in the eyelid tips at 15.5 dpc and had increased in number by 16.0 dpc. In contrast, the assembly of such structures was minimal in most ROCK-I$^{-/-}$ embryos at 15.5 or 16.0 dpc, although a few actin bundles were detected in some of the mutant embryos at 16.0 dpc (Fig. 4 H).

Given that ROCK regulates the phosphorylation of MLC both directly and indirectly in vitro (Amano et al., 2000), we next examined MLC phosphorylation in the eyelid epithelial sheet by staining sections of the eyelid at 16.0 dpc with antibodies specific for phosphorylated MLC (Matsumura et al., 1998). Myosin itself was uniformly stained throughout the eyelid epithelium with no difference between wild-type and ROCK-I$^{-/-}$ embryos (unpublished data). However, whereas staining for phosphorylated MLC was pronounced and associated with actin cables in the eyelid epithelial sheet of wild-type embryos, it was markedly reduced in ROCK-I$^{-/-}$ embryos (Fig. 4 I). We also prepared rabbit polyclonal antibodies to mouse ROCK-I in order to examine ROCK-I distribution during eyelid closure. Immunofluorescence staining with these antibodies revealed the presence of ROCK-I in the eyelid epithelial sheet and skin of wild-type embryos but not in ROCK-I$^{-/-}$ embryos (Fig. 4 J). A prominent ROCK-I signal was apparent in the eyelid epithelial sheet. However, staining was not specifically increased in the cells containing the actomyosin cables but rather was ubiquitous in the eyelid epithelial cells. These results suggest that local ROCK-I activation, rather than the expression level of ROCK-I, regulates the assembly of actomyosin cables during eyelid closure. Together, these observations indicate that phosphorylation of MLC occurs in a ROCK-I–dependent manner in the eyelid epithelial sheet and that this phosphorylation is required for extension of the eyelid epithelial sheet and eyelid closure.

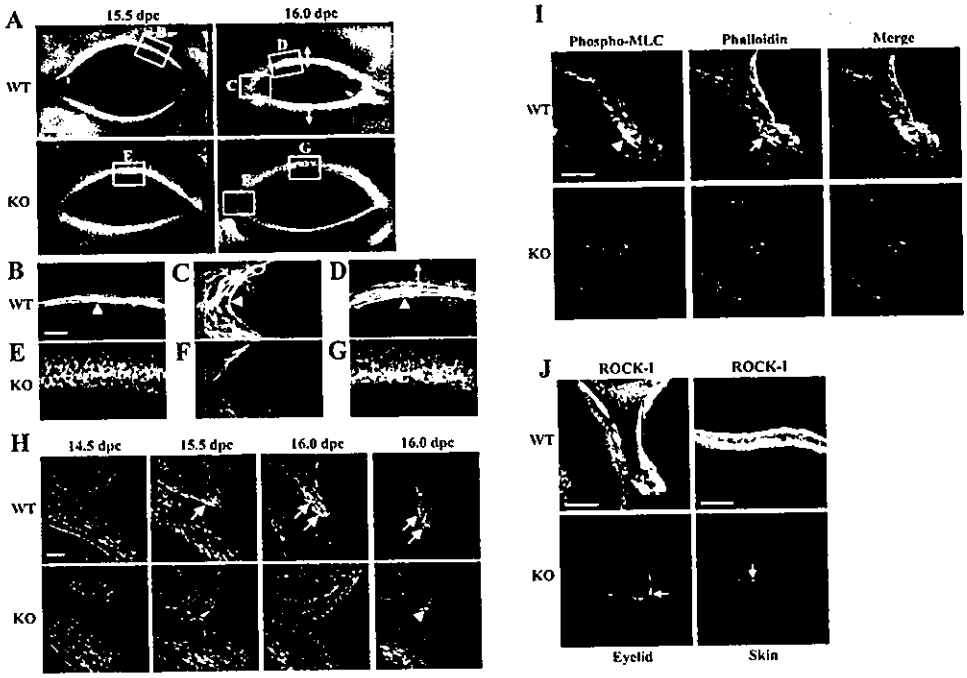

Figure 4. **ROCK-I–dependent formation of actomyosin cables in the eyelid epithelial sheet.** (A) Whole-mount phalloidin staining of the eyelids of wild-type (top) and ROCK-I$^{-/-}$ (bottom) embryos at 15.5 and 16.0 dpc. Bidirectional arrows indicate extension of the eyelid epithelial sheet. Bar, 500 μm. (B–G) Higher magnification views of the boxed regions in A. Arrowheads indicate actin cables in the eyelid epithelial sheet of wild-type embryos. Bidirectional arrows indicate extension of the eyelid epithelial sheet. ROCK-I$^{-/-}$ embryos failed to assemble continuous actin cables. Bar, 50 μm. (H) Phalloidin staining of transverse sections of the eyelid rim of wild-type (top) and ROCK-I$^{-/-}$ (bottom) embryos from 14.5 to 16.0 dpc. A substantial number of actin cables was apparent in a few layers of the eyelid epithelial sheet of wild-type embryos (arrows). Little filamentous-actin accumulation was detected in mutant embryos, with the exception of a few actin bundles in some embryos (arrowhead). Bar, 50 μm. (I) Immunofluorescence staining for phosphorylated MLC (green) and phalloidin staining (red) in sections of the eyelid of wild-type (top) and ROCK-I$^{-/-}$ (bottom) embryos at 16.0 dpc. Phosphorylated MLC was enriched in the eyelid epithelial sheet of wild-type embryos (arrowhead), where it was colocalized with actin cables (arrow). Little phosphorylated MLC staining was detected in ROCK-I$^{-/-}$ embryos. Bar, 50 μm. (J) Immunofluorescence staining for ROCK-I in sections of the eyelid (left) and skin (right) of wild-type (top) and ROCK-I$^{-/-}$ (bottom) embryos at 16.0 dpc. Nonspecific signals are indicated by arrows. Bars, 50 μm.

ROCK-I mediates MLC phosphorylation induced by EGF in primary keratinocytes

Studies with several lines of mutant mice have implicated EGF signaling in eyelid closure (Miettinen et al., 1995; Sibilia and Wagner, 1995; Threadgill et al., 1995). Therefore, we next examined the role of ROCK-I in EGF signaling in primary keratinocytes. Primary keratinocytes were isolated from wild-type and ROCK-I$^{-/-}$ embryos at 18.5 dpc and their identity was confirmed by staining for keratin 5; the presence or absence of ROCK-I, respectively, was also confirmed by immunoblot and immunofluorescence analyses (unpublished data). Measurement of the incorporation of BrdU revealed that the proliferation capacity of the ROCK-I$^{-/-}$ keratinocytes did not differ from that of the wild-type cells (Fig. 5 A), consistent with our Ki67 immunostaining data (Fig. 3 C).

Phalloidin staining showed the presence of actin filaments around the circumference of serum-deprived wild-type keratinocytes (Fig. 5 B); a few short actin bundles were also detected inside the cells. Serum-deprived ROCK-I$^{-/-}$ keratinocytes also contained circumferential actin filaments and short actin bundles. Stimulation of wild-type cells with EGF (10 ng/ml) resulted in the formation of thick actin bundles that resembled stress fibers and spanned the cell length. These actin bundles were observed in 33 and 56.4% of wild-type cells at 30 and 120 min, respectively (Fig. 5, B and C). Similar structures were also induced by EGF in ROCK-I$^{-/-}$ cells, but they were thinner and fewer in number. In addition, only 11 and 20% of ROCK-I$^{-/-}$ cells contained the actin bundles at 30 and 120 min, respectively. These results suggest that ROCK-I plays an important role in the EGF-induced formation of stress fibers in keratinocytes. The EGF-induced formation of actin bundles in both wild-type and ROCK-I$^{-/-}$ cells was prevented by the ROCK inhibitor Y-27632 (Fig. 5 B), suggesting that ROCK-II also contributes to this process.

Given that ROCK acts downstream of Rho, we next examined the possible effect of EGF stimulation on Rho activity in primary keratinocytes with the use of a pull-down assay for the GTP-bound (active) form of Rho. EGF induced a small but reproducible increase in the amount of the GTP-bound form of Rho in both wild-type and ROCK-I$^{-/-}$ keratinocytes (Fig. 5 D). Together, these results thus indicate that the Rho–ROCK signaling pathway is activated by EGF in primary keratinocytes. To elucidate the signaling events downstream of ROCK-I in

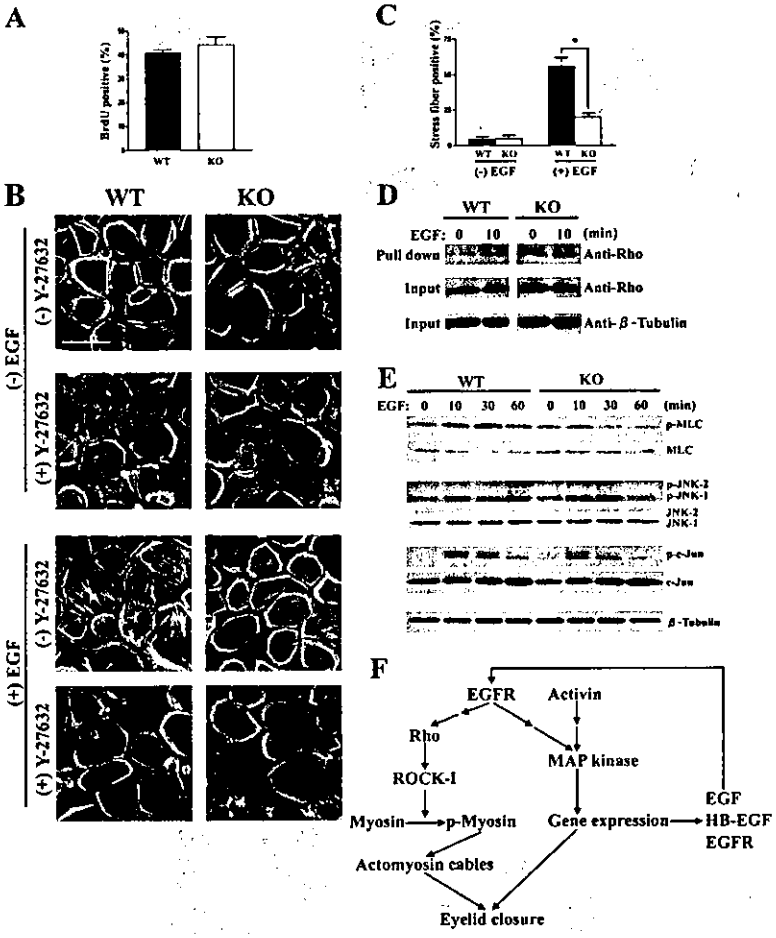

Figure 5. **Impairment of EGF-induced formation of actin stress fibers in primary keratinocytes derived from ROCK-I$^{-/-}$ embryos.** (A) Cell proliferation. Primary keratinocytes derived from wild-type or ROCK-I$^{-/-}$ embryos were cultured in the presence of EGF (10 ng/ml) and evaluated for cell proliferation by measurement of incorporation of BrdU. Data are expressed as the percentage of cells that were BrdU positive and are means ± SEM of values from five independent experiments. (B) Phalloidin staining of keratinocytes. Wild-type and ROCK-I$^{-/-}$ keratinocytes were maintained in serum-free medium for 24 h, cultured with or without EGF (10 ng/ml) for 2 h in the absence or presence of 10 μM Y-27632, and then subjected to staining with phalloidin. Bar, 50 μm. (C) Quantitative analysis of EGF-induced stress fiber formation. Cells incubated with or without EGF for 2 h and stained with phalloidin as in B were analyzed for determination of the percentage of cells with stress fibers. A total of 100 cells were examined for each condition. Data are means ± SEM of values from five independent experiments. *, $P < 0.05$. (D) EGF-induced Rho activation. Wild-type and ROCK-I$^{-/-}$ keratinocytes were cultured in serum-free medium for 24 h, stimulated with EGF (10 ng/ml) for 0 or 10 min, and then subjected to a pull-down assay for the GTP-bound (active) form of Rho. Rho-GTP precipitated from cell lysates was detected by immunoblot analysis with antibodies to Rho (top), and cell lysates (input) were similarly analyzed for the total amounts of Rho (middle) and β-tubulin (bottom). (E) EGF-induced MLC, JNK, and c-Jun phosphorylation. Wild-type and ROCK-I$^{-/-}$ keratinocytes were maintained in serum-free medium for 24 h before stimulation with EGF (10 ng/ml) for the indicated times. Cell lysates were then subjected to immunoblot analysis with antibodies to MLC, to phosphorylated (p-) MLC, to JNK, to phosphorylated JNK, to c-Jun, to phosphorylated c-Jun, and to β-tubulin (control). (F) Proposed role for ROCK-I in mouse eyelid closure. A Rho–ROCK-I–myosin cascade triggered by activation of the EGFR is required for the assembly of the purse stringlike actin cables that contribute to extension of the eyelid epithelial sheet. An autocrine–paracrine pathway mediated by EGFR or activin results in activation of a MAPK cascade and consequent transcription of EGF, heparin-binding EGF (HB-EGF), and EGFR genes.

EGF signaling in these cells, we examined MLC phosphorylation and the activation of c-Jun NH_2-terminal kinase (JNK) and c-Jun. The basal level of MLC phosphorylation did not differ between wild-type and ROCK-I$^{-/-}$ keratinocytes (Fig. 5 E). EGF induced a rapid and transient increase in the extent of MLC phosphorylation in wild-type keratinocytes; this effect was detectable at 10 and 30 min but no longer at 60 min. EGF-induced phosphorylation of MLC was also apparent in ROCK-I$^{-/-}$ keratinocytes at 10 min, but its extent was markedly reduced compared with that observed in wild-type cells. Moreover, MLC phosphorylation in the mutant cells had returned to the basal level by 30 min. In contrast, EGF induced the phosphorylation of JNK, as well as that of its substrate c-Jun, to similar extents in wild-type and ROCK-I$^{-/-}$ keratinocytes (Fig. 5 E). This latter finding was supported by immunofluorescence staining that revealed similar levels of c-Jun and phosphorylated c-Jun in the eyelid epithelial cells of both wild-type and ROCK-I$^{-/-}$ littermates at 16.0 dpc (unpublished data).

Impaired umbilical ring closure in ROCK-I$^{-/-}$ mice

The other major phenotype of ROCK-I$^{-/-}$ mice was omphalocele, herniation of the gut and liver through the umbilical ring in neonates (Fig. 6 A). The umbilical ring was open in wild-type embryos at 15.5 dpc, and the midgut loop protruded through the umbilical ring from the abdominal cavity (Fig. 6 B). The sac of this physiological hernia consisted of an internal lining of peritoneum and an external covering of amnion. ROCK-I$^{-/-}$ mice also showed the physiological umbilical hernia at this stage. By 16.5 dpc, the umbilical ring had closed and the gut had returned to the abdominal cavity in wild-type embryos. In contrast, the umbilical hernia persisted in ROCK-I$^{-/-}$ embryos at this time, resulting in varying degrees of omphalocele in neonates. A ridge-like structure that appeared to constrict the ventral abdominal wall at the site of entry of the umbilical cord was evident in wild-type embryos but not in ROCK-I$^{-/-}$ embryos (Fig. 6 A). Histological analysis revealed that this ridge consisted of

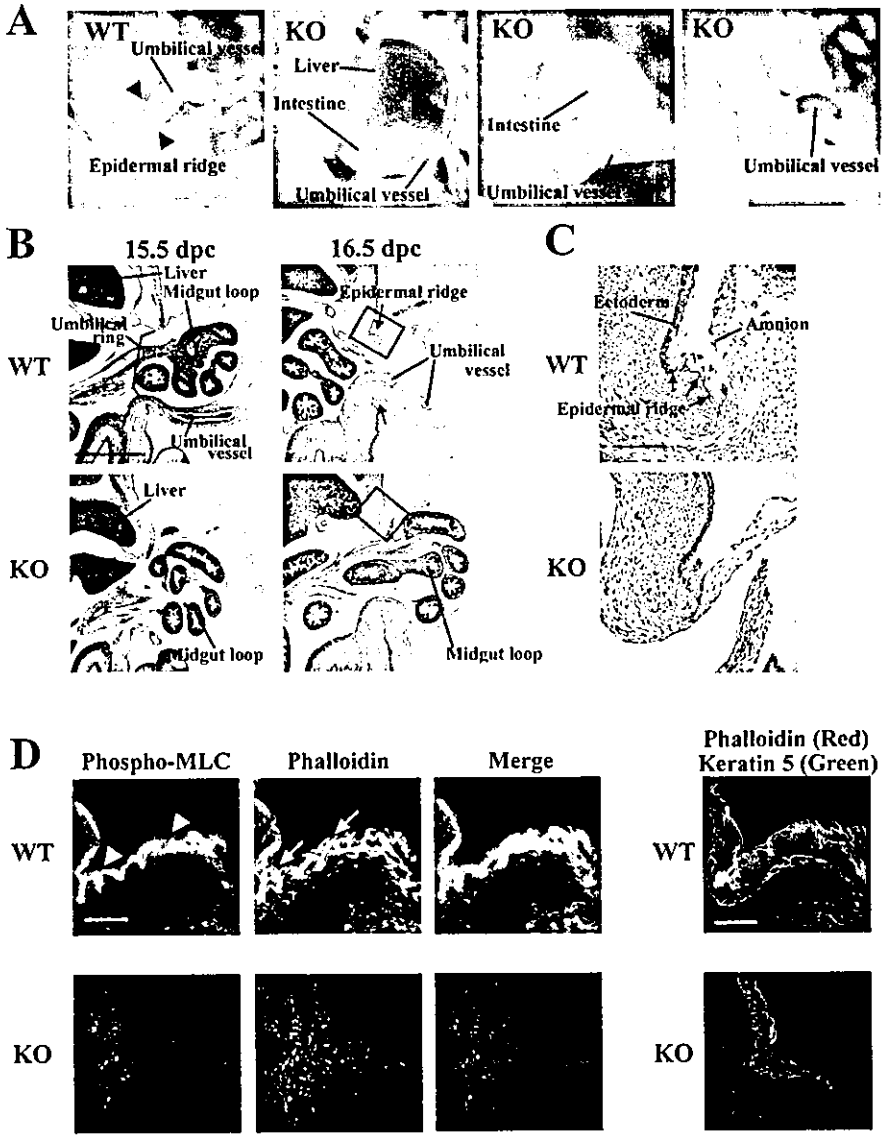

Figure 6. **Impaired closure of the umbilical ring in ROCK-I$^{-/-}$ mice.** (A) Omphalocele in ROCK-I$^{-/-}$ embryos. Wild-type and ROCK-I$^{-/-}$ embryos at 18.5 dpc are shown. Severe, moderate, and mild forms of omphalocele are apparent in the mutant mice shown in the center left, center right, and right panels, respectively. Arrowheads indicate the epidermal ridge in the wild-type embryo. (B) Hematoxylin-eosin staining of sagittal sections through the umbilical region of wild-type (top) and ROCK-I$^{-/-}$ (bottom) embryos at 15.5 (left) and 16.5 (right) dpc. Boxes indicate the region of the ectodermal–amnion transition. Arrows indicate the epidermal ridge. Bar, 1 mm. (C) Higher magnification images of the boxed regions in B. Arrows indicate the epidermal ridge in the wild-type embryo. Bar, 200 μm. (D) Staining of the epidermal ridge. Sections of the epidermal ridge of wild-type (top) and ROCK-I$^{-/-}$ (bottom) embryos at 16.5 dpc were stained with an antibody to phosphorylated MLC (green, arrowheads) and phalloidin (red, arrows) in the left panels, and with phalloidin (red) and an antibody to keratin 5 (green) in the right panel. Bars, 50 μm.

the epidermis and was apparent at the transition between the embryo ectoderm and the amnion of wild-type mice at 16.5 dpc (Fig. 6, B and C). To characterize the function of the epidermal ridge, we stained it for F-actin, phosphorylated MLC, and keratin 5 (Fig. 6 D). Intense phalloidin staining and phosphorylated MLC was detected in the epithelial layer covering the ridge of wild-type embryos. Both of these signals were absent in the epithelium of ROCK-I$^{-/-}$ embryos. These results indicate that specific actin bundles are localized in the epithelial cells of the umbilical ring. Together, these results suggest that the impaired closure of the umbilical ring in ROCK-I$^{-/-}$ embryos is due to failure of myosin phosphorylation and actin assembly in the epithelium at the site of formation of the epidermal ridge at the ectoderm–amnion transition.

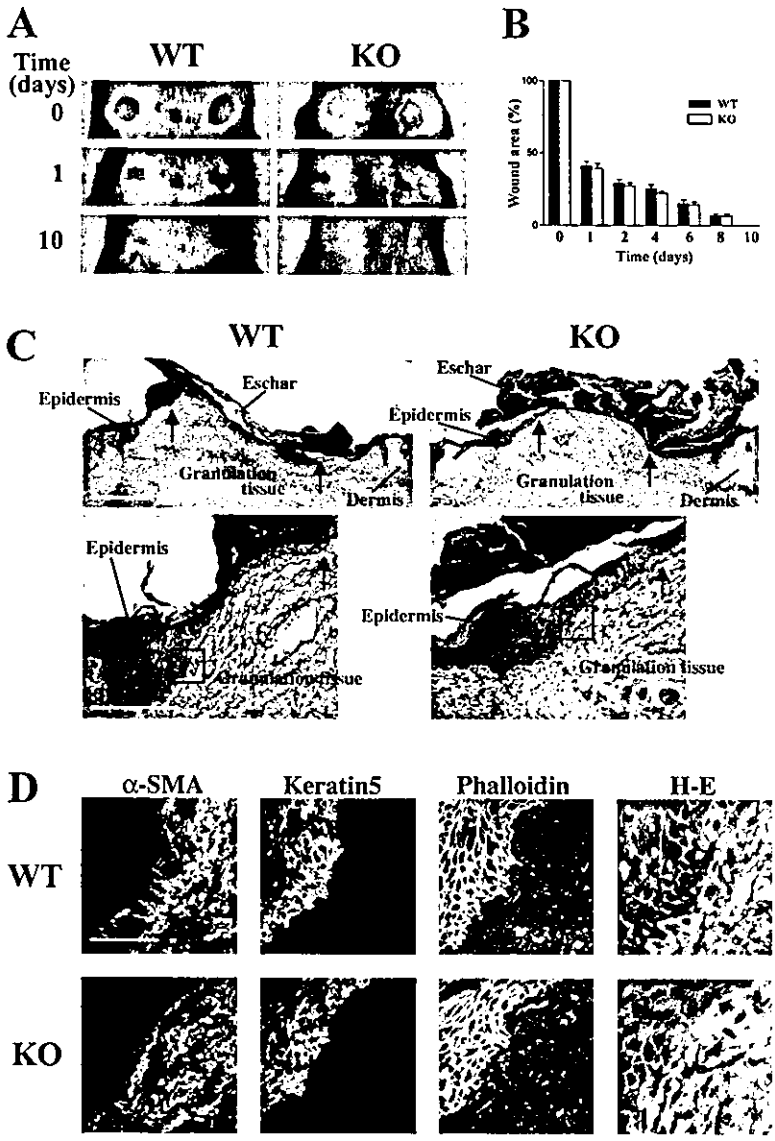

Figure 7. **Wound healing in adult wild-type and ROCK-I$^{-/-}$ mice.** (A) Adult wild-type or ROCK-I$^{-/-}$ mice were shaved on their backs and a 6-mm-diam cylinder of skin (full thickness) was punched out bilaterally. Healing of the wounds was monitored for 10 d. (B) Wound area was expressed as a percentage of the initial value. Quantitative data are means ± SEM (n = 8 wounds for each group). (C) Hematoxylin-eosin staining of the transverse sections of the wound on day 5 from wild-type (left) and ROCK-I$^{-/-}$ mice (right). Arrows indicate the foremost tips of the migrating epithelial sheet. Areas of the migrating epithelial sheet are enlarged in the bottom panels. Bars: (top) 500 μm; (bottom) 200 μm. (D) Staining of the wound edge. Serial sections of the wound from wild-type (top) and ROCK-I$^{-/-}$ (bottom) mice were stained with antibodies to α-SMA, keratin 5, phalloidin, and hematoxylin-eosin (H-E). The fields of view shown correspond to the regions boxed in C. Bar, 50 μm.

Wound healing in adult ROCK-I$^{-/-}$ mice

Finally, we examined the effect of ROCK-I deficiency on wound healing in adult mice. We punched out a full-thickness piece of skin and monitored closure of the excision wound in both wild-type and ROCK-I$^{-/-}$ animals. No apparent repair defect was detected in ROCK-I$^{-/-}$ mice, with wound healing after a time course similar to that observed in wild-type controls (Fig. 7, A and B). Histological examination of the wound on day 5 revealed that the epidermal edges of the wound migrate forward to cover the denuded wound surface in ROCK-I$^{-/-}$ mice as in wild-type controls (Fig. 7 C, arrows). In both groups, myofibroblasts expressing α-smooth muscle actin (α-SMA) were detected underneath the migrating epidermis in granulation tissue (Fig. 7 D). These myofibroblasts was similarly stained with phalloidin in the two groups. These results suggest that ROCK-I is not essential for migration of keratinocytes and appearance of myofibroblasts in adult wound healing process.

Discussion

We have disrupted the gene for ROCK-I, one of the two isoforms of ROCK, by homologous recombination in mice in order to elucidate the functions of this protein in vivo. Mice homozygous for the disrupted ROCK-I allele manifested the EOB and omphalocele phenotypes. Analysis of the molecular mechanisms responsible for these abnormalities has revealed an evolutionarily conserved role of ROCK-I in animal development.

ROCK-I-dependent assembly of actomyosin cables: conservation in mammalian eyelid closure and in *Drosophila* dorsal closure

Monitoring of the morphological changes associated with eyelid closure revealed that the extension of the eyelid epithelial sheet that occurs in wild-type embryos was markedly impaired in ROCK-I$^{-/-}$ mice. Staining with phalloidin and antibodies to phosphorylated MLC revealed the presence of thick actomyosin cables that course around the circumference of the eye and join neighboring cells together in the eyelid epithelial sheet of wild-type mice. This actomyosin structure was specifically lost in the eyelids of ROCK-I$^{-/-}$ mice. Given the functions of ROCK in actomyosin dynamics, these findings indicate that ROCK-I is activated in cells of the eyelid epithelial sheet, catalyzes MLC phosphorylation, and thereby triggers the cross-linking of actin filaments and the assembly of actomyosin bundles, the latter of which then contract and provide the driving force necessary for eyelid closure. The loss of such ROCK-I function is thus the likely cause of the EOB phenotype in ROCK-I$^{-/-}$ mice.

This process that we propose for eyelid closure is similar to that which underlies dorsal closure of the fly epidermis (Jacinto et al., 2002). In both instances, the epithelium extends as a sheet and actomyosin cables are present in these sheets. On the basis of the contribution of a MAPK cascade (see below) to both processes, Xia and Karin (2004) suggested the operation of an evolutionarily conserved mechanism both in dorsal closure in *Drosophila* and in eyelid closure in mammals. Consistent with this proposal and with our present findings, genetic analysis in *Drosophila* has implicated the Rho pathway in dorsal closure (Harden et al., 1999; Magie et al., 1999). Moreover, disruption of the *Drosophila* gene for the myosin binding subunit of myosin phosphatase resulted in impairment of dorsal closure (Mizuno et al., 2002). Given that the myosin binding subunit of myosin phosphatase is the major substrate of ROCK in its indirect regulation of phosphorylated MLC, this finding suggests the participation of ROCK in dorsal closure. Laser-ablation experiments have shown that the actin cables generate the contractile force responsible for movement of the epithelial sheet during dorsal closure, functioning in a manner analogous to a purse string (Kiehart et al., 2000; Hutson et al., 2003). Therefore, we propose that actomyosin cable in eyelid epithelial sheet contracts like a purse string, and thus drive the eyelid epithelial sheet movement forward as seen in dorsal closure. In addition to dorsal closure, purse stringlike actin assembly occurs at the margin of wounds in chick embryos, and experiments with C3 exoenzyme have indicated that Rho mediates this assembly (Brock et al., 1996; Wood et al., 2002). Therefore, it is likely that Rho–ROCK signaling also contributes to wound closure in chick embryos. Thus, ROCK-mediated assembly and contraction of actomyosin cables appears to be an evolutionarily conserved mechanism for tissue closure.

In contrast to the findings in chick embryos, we found that ROCK-I deficiency did not affect wound closure in adult mice. Wound healing in adult skin is a complex process. After wounding, a fibrin clot and then granulation tissue form in the wound, after which a sheet of keratinocytes migrates from the wound edges to repair the epidermal layer (Martin, 1997). This migration of the epithelium occurs by integrin-dependent extension of lamellipodia over the ECM. Failure of ROCK-I deficiency to block this process suggests that ROCK-I is not required for cell migration over ECM in adult skin. Consistent with this conclusion, an in vitro assay of wound healing with a monolayer of cultured keratinocytes revealed that keratinocytes derived from wild-type or ROCK-I$^{-/-}$ mice migrated in response to EGF stimulation in similar manners (unpublished data).

Role of ROCK-I in EGF signaling during eyelid closure

EGFR-deficient mice (Miettinen et al., 1995; Sibilia and Wagner, 1995; Threadgill et al., 1995) exhibit an EOB phenotype similar to that of ROCK-I$^{-/-}$ mice. In addition, mice deficient in TGF-α (Luetteke et al., 1993; Mann et al., 1993), an EGFR ligand, and mice deficient in Gab1 (Itoh et al., 2000), an adaptor molecule of the EGFR, also manifest the open-eye phenotype, suggesting that EGFR signaling is critical for eyelid closure. The EGFR is activated in the same region of the eyelid epithelial sheet (Li et al., 2003) as that found to contain actomyosin cables in the present study. Given that Rho is activated by EGFR signaling in cultured cells (Ridley and Hall, 1992), Rho–ROCK signaling likely functions downstream of the EGFR in eyelid closure. We have now shown that EGF activates Rho and induces both phosphorylation of MLC and formation of stress fibers in a ROCK-I–dependent manner in primary mouse keratinocytes, supporting the notion that ROCK-I functions in induction of formation of the actomyosin cables in the eyelid epithelial sheet.

We also examined whether the Rho–ROCK pathway might play a role in EGFR signaling other than that which leads to the formation of actomyosin cables. Knockout mouse studies have implicated a MAPK cascade in EGF signaling during eyelid closure. For example, MEKK1-deficient mice exhibit the EOB phenotype (Zhang et al., 2003). JNK1$^{+/-}$/JNK2$^{-/-}$ mice (Weston et al., 2004) as well as mice with keratinocyte-specific knockout of c-Jun (Li et al., 2003; Zenz et al., 2003) are also defective in eyelid closure. In all of these mutant mice, the EOB phenotype is associated with reduced expression of the EGFR ligands EGF or heparin-binding EGF, indicating the presence of a positive feedback loop. The recent observation that RhoA stimulates the expression of c-Jun by activating JNK (Marinissen et al., 2004) led us to examine the possible role of ROCK-I in this signaling cascade. However, JNK activation and phosphorylation of c-Jun were not altered in ROCK-I$^{-/-}$ keratinocytes, excluding a role for ROCK-I in this MAPK cascade. On the basis of these various observations, we propose the model shown in Fig. 5 F for the role of ROCK-I in the EGFR signaling associated with eyelid closure.

Umbilical ring closure is mediated by ROCK-I-dependent actin assembly

A reduced level of MLC phosphorylation and consequent failure of actomyosin assembly in the epithelium may also explain the omphalocele phenotype of ROCK-I$^{-/-}$ neonates. Accumu-

lation of filamentous-actin and MLC phosphorylation were observed in the epithelial cells at the ectoderm–amnion transition that formed a ridge-shaped structure encircling the umbilical ring in wild-type mouse embryos. Neither such filamentous-actin accumulation nor MLC phosphorylation was detected and the epidermal ridge was not formed in ROCK-I$^{-/-}$ embryos. In contrast, although omphalocele can be caused by defects or malformation of the ventral body wall itself (Eggenschwiler et al., 1997; Zhang et al., 1997; Brewer and Williams, 2004), this structure was intact in ROCK-I$^{-/-}$ embryos. These results indicate that ROCK-I$^{-/-}$ embryos are defective in the final step of umbilical ring closure, which we propose is executed by ROCK-I–mediated actomyosin contraction of the epithelium in the epidermal ridge. In contrast to the EOB phenotype, omphalocele is not observed in mice defective in EGFR signaling. Moreover, the extents of the EOB phenotype and of omphalocele were not correlated in ROCK-I$^{-/-}$ embryos, suggesting that the upstream signaling in umbilical closure differs from that in eyelid closure. The omphalocele phenotype of the ROCK-I$^{-/-}$ mice is reminiscent of that of human neonatal omphalocele, for which failure of umbilical ring closure is proposed as a major cause. The incidence of human omphalocele has been estimated as 1 in 4,000–7,000 live births (Weber et al., 2002). Characterization of the detailed mechanism of the failure of umbilical ring closure in ROCK-I$^{-/-}$ mice may thus provide insight into the pathophysiology of omphalocele and its treatment in humans.

Further considerations

Given the importance of ROCK in Rho signaling, the phenotype of ROCK-I$^{-/-}$ mice described in the present study as well as that of ROCK-II$^{-/-}$ mice we described previously (Thumkeo et al., 2003) might be considered milder than expected. Both types of knockout mice manifest perinatal problems, but those that survive develop in an apparently normal manner to adulthood. In addition, in the present study, some ROCK-I$^{-/-}$ embryos exhibited partial extension of the eyelid epithelial sheet and associated actin bundling. EGF induced a low level of stress fiber formation in ROCK-I$^{-/-}$ keratinocytes, and this effect was abolished by Y-27632, suggesting a contribution, albeit little, by ROCK-II in the same process. Consistently, we recently found that a substantial proportion of ROCK-II$^{-/-}$ embryos also exhibited the EOB phenotype and omphalocele (unpublished data). These results suggest that ROCK-I and ROCK-II function in a redundant manner, and indicate a possibility that each is able to compensate functionally for the loss of the other in most systems without up-regulation except the tissues such as the placenta (Thumkeo et al., 2003) and the eyelid and umbilical ring (this study). The generation of double knockout mice deficient in both ROCK-I and ROCK-II should therefore provide further insight into the role of the ROCK family of kinases in development.

Materials and methods

Generation of ROCK-I–deficient mice

Several clones containing various portions of the ROCK-I gene were isolated from a 129/SvJ lambda FIXII genomic library (Stratagene). A 1.1-kb fragment containing the first 3 bp and 5′ flanking region of exon 3 was generated by PCR with a 3.8-kb genomic DNA fragment containing exons 3 and 4 as the template and with a forward primer containing a SmaI site and a reverse primer containing a ClaI site. The amplified fragment was subcloned as a short arm into pBluescript SK+ (Stratagene). The plasmid DNA was cut with ClaI and SalI and fused with a ClaI–SalI fragment containing the β-galactosidase gene. The multicloning site of pKOScrambler915 (Stratagene) was modified to contain the restriction enzyme sites RsrII–EcoRI–XhoI–AscI–SacII–ClaI–SmaI–BglII–AvrII–SalI–NotI, yielding mpKO915. The latter plasmid was cut with AscI, and the AscI fragment of the phosphoglycerate kinase promoter-neomycin resistance (neo) cassette was introduced at this site. The diphtheria toxin A gene was then inserted at the RsrII site of the mpKO915 plasmid, after which the SmaI–SalI fragment containing the short arm of the ROCK-I gene and the β-galactosidase gene from pBluescript SK+ was subcloned into the EcoRI–XhoI site. Finally, a 7.8-kb EcoRV–NheI fragment of genomic DNA of ROCK-I was inserted as the long arm into the SmaI site of the vector to generate the targeting construct (Fig. 1 A). The targeting vector was linearized with NotI and introduced into embryonic stem cells (line RW4; Genome System) by electroporation. G418-resistant clones were isolated, and homologous recombination was verified in three clones by PCR-based genotyping. Cells of each of the three clones were injected into blastocysts, and the chimeric male offspring obtained were mated with C57BL/6N females. ROCK-I$^{+/-}$ heterozygous mice were then intercrossed to produce ROCK-I$^{-/-}$ homozygotes. Mice studied in the present work had been backcrossed to the C57BL/6N strain for more than five generations. The morning of the day on which a vaginal plug was detected was designated as 0.5 dpc. All animal experiments were approved by the Committee on Animal Research of Kyoto University Faculty of Medicine and were performed according to the guidelines for the protection of experimental animals of Kyoto University, Kyoto, Japan.

Genotyping

Genotyping was performed by Southern blot or PCR analysis with genomic DNA isolated from embryonic stem cells, embryonic visceral yolk sacs, or the tail of mice. For Southern analysis, 10 μg of genomic DNA were digested with BglII for 12 h at 37°C, and the resulting fragments were fractionated by electrophoresis on a 0.7% agarose gel, transferred to a Hybond-N$^+$ nylon membrane (Amersham Biosciences), and subjected to hybridization overnight at 42°C in hybridization buffer (Ultrasensitive Hybridization buffer; Ambion) with the external probe (Fig. 1 A) that had been randomly labeled with α-[^{32}P]dCTP (1×10^6 to 2×10^6 cpm/ml) with the use of Ready-To-Go DNA Labeling Beads (Amersham Biosciences). For PCR analysis, the primers were 5′-CACTACAATCAAGTAAGCTTCATCC-3′ (forward primer for the wild-type and targeted allele), 5′-GCTGAGCAGCTTCATAGCATAAACC-3′ (reverse primer for the wild-type allele), and 5′-GACCAGACCGTTCATACAGAACTGG-3′ (reverse primer for the targeted allele).

Production of antibodies to mouse ROCK-I

A GST fusion protein of fragment 1b of mouse ROCK-I (amino acids 400–662) was produced in *Escherichia coli* BL21 cells, and purified with the use of glutathione-Sepharose 4B beads (Amersham Biosciences). GST was cleaved, and ROCK-I (1b) was used as the antigen and injected into rabbits. Specific antibodies to mouse ROCK-I were then affinity purified from serum with the use of ROCK-I (1b) immobilized on CNBr beads (Amersham Biosciences).

Immunoblot analysis

The entire brain of adult mice or confluent monolayers of primary keratinocytes were homogenized, and used for immunoblotting as described previously (Thumkeo et al., 2003) with antibodies to either ROCK-I, ROCK-II (H-85; Santa Cruz Biotechnology, Inc.), β-tubulin (TUB 2.1; Sigma-Aldrich), phosphorylated MLC (Matsumura et al., 1998), MLC (A-10; Santa Cruz Biotechnology, Inc.), phosphorylated JNK (Promega), JNK (BD Biosciences), phosphorylated c-Jun (Cell Signaling Technology), or c-Jun (H-79; Santa Cruz Biotechnology, Inc.).

Whole-mount staining for β-galactosidase

Embryos isolated at 13.5 or 15.5 dpc were processed for whole-mount β-galactosidase staining as described previously (Thumkeo et al., 2003).

Histological and immunofluorescence analyses

Samples were fixed in 10% formaldehyde, dehydrated with a graded series of ethanol solutions, and embedded in paraffin. 8-μm sections were prepared, subjected to removal of paraffin by immersion in xylene, rehy-

drated, and stained with hematoxylin-eosin. The samples were embedded in Tissue Tek OCT compound (Sakura) and frozen on dry ice. Cryostat sections (12 μm) were prepared and subjected to indirect immunofluorescence analysis with antibodies to either phosphorylated MLC (Matsumura et al., 1998), myosin (BT-561; Biomedical Technologies), keratin 5 or keratin 10 (BabCo), keratin 6 (McGowan and Coulombe, 1998), Ki67 (Novocastra), or α-SMA (1A4; Sigma-Aldrich). Antibody to keratin 6 was a gift from B.A. Coulombe (Johns Hopkins University of Medicine, Baltimore, MD). Immunocomplexes were detected with Alexa Fluor 488–conjugated donkey antibodies to rabbit or mouse IgG (Molecular Probes). TOPRO-3 iodide and phalloidin labeled with either Oregon green or Texas red (Molecular Probes) were used for staining of nuclei and filamentous actin, respectively. Primary keratinocytes were fixed with 4% PFA for 15 min at RT, permeabilized for 5 min with PBS containing 0.1% Triton X-100, and stained for filamentous actin with Oregon green phalloidin. Specimens were examined with the LSM 510 confocal microscope, at RT, with both 40× (Plan-Neofluor; NA 1.3) and 63× (Plan-Apochromat; NA 1.4) objective lens. Images were acquired with LSM 510 AIM software (Carl Zeiss MicroImaging, Inc.). All pseudo-color representations were assembled using Adobe Photoshop version 6.0 for illustrative purpose only.

Scanning electron microscopy

The head of embryos at 14.5–16.5 dpc was fixed in 0.1 M sodium phosphate buffer, pH 7.4, containing 1% glutaraldehyde and 4% formaldehyde, washed with 0.1 M sodium phosphate buffer containing 0.1 M sucrose, and dehydrated with a graded series of ethanol solutions. Specimens were then dried and sputter coated according to standard procedures before examination with an S4700 scanning electron microscope (Hitachi).

Whole-mount phalloidin staining

Eyelids isolated together with the skin around the eye from embryos at 15.5 or 16.0 dpc were fixed in 4% PFA for 30 min, washed with PBS, incubated for 1 h with 200 μl of Oregan green phalloidin diluted 1:50 in PBS containing 0.2% Triton X-100, and washed five times with the PBS Triton X-100 solution. Specimens were examined under a fluorescence microscope (model BX50; Olympus) equipped with a charge-coupled device camera (model DP-70; Olympus) as well as with the LSM 510 confocal imaging system (Carl Zeiss MicroImaging, Inc.).

Primary culture of keratinocytes

Primary culture of mouse keratinocytes was performed as described previously (Sano et al., 1999). For pull-down assay, keratinocytes were lysed in pull-down lysis buffer (Upstate Biotechnology), and the lysate was subjected to the pull-down assay using a GST fusion protein containing the Rho binding domain of Rhotekin (Upstate Biotechnology). For BrdU incorporation, keratinocytes were cultured for 24 h with EGF (10 ng/ml), after which BrdU (Roche) was added to the culture medium at 10 μM. After further incubation for 1 h, the cells were fixed and stained with antibodies to BrdU (BMC 9318; Roche).

We thank P.A. Coulombe for polyclonal antibodies to keratin 6; S. Itami and Y. Sumikawa for protocols and advice on primary culture of keratinocytes; M. Fujioka for scanning electron microscopy; Y. Andou for help with preparation of the polyclonal antibodies to ROCK-I; T. Fujiwara, K. Nonomura, Y. Che, and K. Hamajima for technical assistance; and T. Arai and Y. Kitagawa for secretarial assistance.

This work was supported in part by a grant-in-aid for Specially Promoted Research from the Ministry of Education, Culture, Sports, Science, and Technology of Japan, a grant from the Organization for Pharmaceutical Safety and Research, and a grant from Mitsubishi Pharma Corporation. The authors declare that they have no competing financial interests.

Submitted: 29 November 2004
Accepted: 3 February 2005

References

Amano, M., Y. Fukata, and K. Kaibuchi. 2000. Regulation and functions of Rho-associated kinase. *Exp. Cell Res.* 261:44–51.

Brewer, S., and T. Williams. 2004. Loss of AP-2alpha impacts multiple aspects of ventral body wall development and closure. *Dev. Biol.* 267:399–417.

Brock, J., K. Midwinter, J. Lewis, and P. Martin. 1996. Healing of incisional wounds in the embryonic chick wing bud: characterization of the actin purse-string and demonstration of a requirement for Rho activation. *J. Cell Biol.* 135:1097–1107.

Eggenschwiler, J., T. Ludwig, P. Fisher, P.A. Leighton, S.M. Tilghman, and A. Efstratiadis. 1997. Mouse mutant embryos overexpressing IGF-II exhibit phenotypic features of the Beckwith-Wiedemann and Simpson-Golabi-Behmel syndromes. *Genes Dev.* 11:3128–3142.

Etienne-Manneville, S., and A. Hall. 2002. Rho GTPases in cell biology. *Nature.* 420:629–635.

Findlater, G.S., R.D. McDougall, and M.H. Kaufman. 1993. Eyelid development, fusion and subsequent reopening in the mouse. *J. Anat.* 183:121–129.

Fuchs, E. 1996. The cytoskeleton and disease: genetic disorders of intermediate filaments. *Annu. Rev. Genet.* 30:197–231.

Harden, N., M. Ricos, Y.M. Ong, W. Chia, and L. Lim. 1999. Participation of small GTPases in dorsal closure of the *Drosophila* embryo: distinct roles for Rho subfamily proteins in epithelial morphogenesis. *J. Cell Sci.* 112:273–284.

Hutson, M.S., Y. Tokutake, M.S. Chang, J.W. Bloor, S. Venakides, D.P. Kiehart, and G.S. Edwards. 2003. Forces for morphogenesis investigated with laser microsurgery and quantitative modeling. *Science.* 300:145–149.

Itoh, M., Y. Yoshida, K. Nishida, M. Narimatsu, M. Hibi, and T. Hirano. 2000. Role of Gab1 in heart, placenta, and skin development and growth factor- and cytokine-induced extracellular signal-regulated kinase mitogen-activated protein kinase activation. *Mol. Cell. Biol.* 20:3695–3704.

Jacinto, A., S. Woolner, and P. Martin. 2002. Dynamic analysis of dorsal closure in *Drosophila*: from genetics to cell biology. *Dev. Cell.* 3:9–19.

Kaufman, M.H. 2002. The Atlas of Mouse Development. Academic Press, London. 525 pp.

Kiehart, D.P., C.G. Galbraith, K.A. Edwards, W.L. Rickoll, and R.A. Montague. 2000. Multiple forces contribute to cell sheet morphogenesis for dorsal closure in *Drosophila*. *J. Cell Biol.* 149:471–490.

Li, G., C. Gustafson-Brown, S.K. Hanks, K. Nason, J.M. Arbeit, K. Pogliano, R.M. Wisdom, and R.S. Johnson. 2003. c-Jun is essential for organization of the epidermal leading edge. *Dev. Cell.* 4:865–877.

Luetteke, N.C., T.H. Qiu, R.L. Peiffer, P. Oliver, O. Smithies, and D.C. Lee. 1993. TGF alpha deficiency results in hair follicle and eye abnormalities in targeted and waved-1 mice. *Cell.* 73:263–278.

Maekawa, M., T. Ishizaki, S. Boku, N. Watanabe, A. Fujita, A. Iwamatsu, T. Obinata, K. Ohashi, K. Mizuno, and S. Narumiya. 1999. Signaling from Rho to the actin cytoskeleton through protein kinases ROCK and LIM-kinase. *Science.* 285:895–898.

Magie, C.R., M.R. Meyer, M.S. Gorsuch, and S.M. Parkhurst. 1999. Mutations in the Rho1 small GTPase disrupt morphogenesis and segmentation during early *Drosophila* development. *Development.* 126:5353–5364.

Mann, G.B., K.J. Fowler, A. Gabriel, E.C. Nice, R.L. Williams, and A.R. Dunn. 1993. Mice with a null mutation of the TGF alpha gene have abnormal skin architecture, wavy hair, and curly whiskers and often develop corneal inflammation. *Cell.* 73:249–261.

Marinissen, M.J., M. Chiariello, T. Tanos, O. Bernard, S. Narumiya, and J.S. Gutkind. 2004. The small GTP-binding protein RhoA regulates c-jun by a ROCK-JNK signaling axis. *Mol. Cell.* 14:29–41.

Martin, P. 1997. Wound healing-aiming for perfect skin regeneration. *Science.* 276:75–81.

Martin, P., and S.M. Parkhurst. 2004. Parallels between tissue repair and embryo morphogenesis. *Development.* 131:3021–3034.

Matsumura, F., S. Ono, Y. Yamakita, G. Totsukawa, and S. Yamashiro. 1998. Specific localization of serine 19 phosphorylated myosin II during cell locomotion and mitosis of cultured cells. *J. Cell Biol.* 140:119–129.

Mazzalupo, S., and P.A. Coulombe. 2001. A reporter transgene based on a human keratin 6 gene promoter is specifically expressed in the periderm of mouse embryos. *Mech. Dev.* 100:65–69.

McGowan, K.M., and P.A. Coulombe. 1998. Onset of keratin 17 expression coincides with the definition of major epithelial lineages during skin development. *J. Cell Biol.* 143:469–486.

Miettinen, P.J., J.E. Berger, J. Meneses, Y. Phung, R.A. Pedersen, Z. Werb, and R. Derynck. 1995. Epithelial immaturity and multiorgan failure in mice lacking epidermal growth factor receptor. *Nature.* 376:337–341.

Mizuno, T., K. Tsutsui, and Y. Nishida. 2002. *Drosophila* myosin phosphatase and its role in dorsal closure. *Development.* 129:1215–1223.

Narumiya, S. 1996. The small GTPase Rho: cellular functions and signal transduction. *J. Biochem. (Tokyo).* 120:215–228.

Ridley, A.J., and A. Hall. 1992. The small GTP-binding protein rho regulates the assembly of focal adhesions and actin stress fibers in response to growth factors. *Cell.* 70:389–399.

Riento, K., and A.J. Ridley. 2003. Rocks: multifunctional kinases in cell behaviour. *Nat. Rev. Mol. Cell Biol.* 4:446–456.

Sano, S., S. Itami, K. Takeda, M. Tarutani, Y. Yamaguchi, H. Miura, K. Yoshikawa, S. Akira, and J. Takeda. 1999. Keratinocyte-specific ablation of Stat3 exhibits impaired skin remodeling, but does not affect skin

morphogenesis. *EMBO J.* 18:4657–4668.

Sibilia, M., and E.F. Wagner. 1995. Strain-dependent epithelial defects in mice lacking the EGF receptor. *Science.* 269:234–238.

Threadgill, D.W., A.A. Dlugosz, L.A. Hansen, T. Tennenbaum, U. Lichti, D. Yee, C. LaMantia, T. Mourton, K. Herrup, R.C. Harris, et al. 1995. Targeted disruption of mouse EGF receptor: effect of genetic background on mutant phenotype. *Science.* 269:230–234.

Thumkeo, D., J. Keel, T. Ishizaki, M. Hirose, K. Nonomura, H. Oshima, M. Oshima, M.M. Taketo, and S. Narumiya. 2003. Targeted disruption of the mouse rho-associated kinase 2 gene results in intrauterine growth retardation and fetal death. *Mol. Cell. Biol.* 23:5043–5055.

Uehata, M., T. Ishizaki, H. Satoh, T. Ono, T. Kawahara, T. Morishita, H. Tamakawa, K. Yamagami, J. Inui, M. Maekawa, and S. Narumiya. 1997. Calcium sensitization of smooth muscle mediated by a Rho-associated protein kinase in hypertension. *Nature.* 389:990–994.

Weber, T.R., M. Au-Fliegner, C.D. Downard, and S.J. Fishman. 2002. Abdominal wall defects. *Curr. Opin. Pediatr.* 14:491–497.

Weston, C.R., A. Wong, J.P. Hall, M.E. Goad, R.A. Flavell, and R.J. Davis. 2004. The c-Jun NH2-terminal kinase is essential for epidermal growth factor expression during epidermal morphogenesis. *Proc. Natl. Acad. Sci. USA.* 101:14114–14119.

Wood, W., A. Jacinto, R. Grose, S. Woolner, J. Gale, C. Wilson, and P. Martin. 2002. Wound healing recapitulates morphogenesis in *Drosophila* embryos. *Nat. Cell Biol.* 4:907–912.

Xia, Y., and M. Karin. 2004. The control of cell motility and epithelial morphogenesis by Jun kinases. *Trends Cell Biol.* 14:94–101.

Zenz, R., H. Scheuch, P. Martin, C. Frank, R. Eferl, L. Kenner, M. Sibilia, and E.F. Wagner. 2003. c-Jun regulates eyelid closure and skin tumor development through EGFR signaling. *Dev. Cell.* 4:879–889.

Zhang, L., W. Wang, Y. Hayashi, J.V. Jester, D.E. Birk, M. Gao, C.Y. Liu, W.W. Kao, M. Karin, and Y. Xia. 2003. A role for MEK kinase 1 in TGF-beta/activin-induced epithelium movement and embryonic eyelid closure. *EMBO J.* 22:4443–4454.

Zhang, P., N.J. Liegeois, C. Wong, M. Finegold, H. Hou, J.C. Thompson, A. Silverman, J.W. Harper, R.A. DePinho, and S.J. Elledge. 1997. Altered cell differentiation and proliferation in mice lacking p57KIP2 indicates a role in Beckwith-Wiedemann syndrome. *Nature.* 387:151–158.

THE JOURNAL OF BIOLOGICAL CHEMISTRY
Vol. 278, No. 20, Issue of May 16, pp. 18597–18605, 2003
Printed in U.S.A.

Molecular Cloning and Characterization of CLICK-III/CaMKIγ, a Novel Membrane-anchored Neuronal Ca^{2+}/Calmodulin-dependent Protein Kinase (CaMK)*

Received for publication, January 17, 2003, and in revised form, February 26, 2003
Published, JBC Papers in Press, March 11, 2003, DOI 10.1074/jbc.M300578200

Sayaka Takemoto-Kimura‡§, Hisashi Terai‡, Maki Takamoto‡¶, Shogo Ohmae‡, Shoko Kikumura‡, Eri Segi‡‖, Yoshiki Arakawa‡§, Tomoyuki Furuyashiki‡‖, Shuh Narumiya‡, and Haruhiko Bito‡¶‡‡**

*From the ‡Department of Pharmacology, Kyoto University Faculty of Medicine, ¶PRESTO-Japan Science and Technology Corporation, Sakyo-ku, Kyoto 606-8315, and **Department of Neurochemistry, University of Tokyo Graduate School of Medicine, Bunkyo-ku, Tokyo 113-0033, Japan*

During a screen for novel putative Ca^{2+}/calmodulin-dependent protein kinase (CaMK)-like CREB kinases (CLICKs), we have cloned a full-length cDNA for CLICK-III/CaMKIγ, an isoform of the CaMKI family with an extended C-terminal domain ending with *CAAX* motif (where *AA* is aliphatic acid). As expected from the similarity of its kinase domain with the other CaMKI isoforms, full activation of CLICK-III/CaMKIγ required both Ca^{2+}/CaM and phosphorylation by CaMKK. We also found that Ca^{2+}/cAMP-response element-binding protein (CREB) was a good substrate for CLICK-III/CaMKIγ, at least *in vitro*. Interestingly enough, CLICK-III/CaMKIγ transcripts were most abundant in neurons, with the highest levels in limited nuclei such as the central nucleus of the amygdala (CeA) and the ventromedial hypothalamus. Consistent with the presence of the *CAAX* motif, CLICK-III/CaMKIγ was found to be anchored to various membrane compartments, especially to Golgi and plasma membranes. Both point mutation in the *CAAX* motif and treatment with compactin, a 3-hydroxy-3-methylglutaryl-coenzyme A reductase inhibitor, disrupted such membrane localization, suggesting that membrane localization of CLICK-III/CaMKIγ occurred in a prenylation-dependent way. These findings provide a novel mechanism by which neuronal CaMK activity could be targeted to specific membrane compartments.

Neuronal Ca^{2+} is known to play a critical role as an intracellular second messenger, linking neuronal excitability with many kinds of cellular biological events including synaptic plasticity and neuronal cell survival/apoptosis (1–4). One of the unique features of Ca^{2+} is that its concentration can be dynamically regulated both temporally and spatially (5). Despite a growing knowledge about the critical molecules involved in neuronal Ca^{2+} influx and mobilization (*e.g. N*-methyl-D-aspartic acid receptors, voltage-gated Ca^{2+} channels, inositol 1,4,5-trisphosphate receptors, and ryanodine receptors), how these are converted to the specific cellular events remains largely unknown.

A significant part of signaling downstream Ca^{2+} is thought to be mediated by calmodulin (CaM),[1] a ubiquitous and evolutionary well conserved intracellular Ca^{2+} receptor (6, 7). Although a large number of molecules have been shown to be targeted and activated by the Ca^{2+}/CaM complex, one subgroup of multifunctional kinases, Ca^{2+}/calmodulin-dependent protein kinases (CaMKs), has been ascribed a prominent role. This is because several unique characteristics of this group of kinases, such as rapid activation by Ca^{2+}, steep Ca^{2+}/CaM dependence, and induction of an autonomous kinase activity following activation, render its members good candidates as molecular devices able to convert a transient burst of synaptic activity into a longer lasting covalent modification of substrate proteins (8–15). Indeed, among the CaMK family members, CaMKIIα and β isoforms, which are present postsynaptically and presynaptically, have been implicated in various kinds of synaptic plasticity and homeostasis (8–11), whereas a CaMKK/CaMKIV cascade has been shown to couple synaptic stimuli with CREB-dependent gene expression (4, 12, 16). The ability of the CaMKI isoforms and a related kinase, CKLiK, to phosphorylate neuronal substrates, such as synapsin I and CREB *in vitro*, has been demonstrated so far (13, 17, 18). However, little is yet known about the physiological role of CaMKI, although CaMKIα and CaMKIβ have been shown to be expressed both in neural as well as non-neural peripheral tissues (13, 17–21).

In this study, we report the molecular cloning of mouse full-length CLICK-III/CaMKIγ (occasionally abbreviated to CLICK-III in this paper), an isoform of CaMKI family, that has a longer C-terminal region terminating with a *CAAX* motif (where *AA* is aliphatic acid). This motif has been shown to be conjugated with isoprenoid lipids, thereby allowing proper tar-

* This work was supported by grants-in-aid from the Ministry of Education, Science, Sports, Culture and Technology, the Ministry of Health, Labor, and Welfare of Japan, a PRESTO investigatorship from the Japan Science and Technology Corp., and grants from the Asahi Glass Foundation, the Human Frontier Science Program, the Narishige Neuroscience Research Foundation, the Tokyo Biochemical Research Foundation, the Ube Research Foundation, and the Yamanouchi Foundation for Research on Metabolic Disorders. The costs of publication of this article were defrayed in part by the payment of page charges. This article must therefore be hereby marked "*advertisement*" in accordance with 18 U.S.C. Section 1734 solely to indicate this fact.

§ Predoctoral fellows from the Japan Society for Promotion of Science.
‖ Postdoctoral fellows from the Japan Society for Promotion of Science.
‡‡ To whom correspondence should be addressed. Tel.: 81-3-5841-3559; Fax: 81-3-3814-8154; E-mail: hbito@m.u-tokyo.ac.jp.

[1] The abbreviations used are: CaM, calmodulin; CaMK, Ca^{2+}/calmodulin-dependent protein kinase; CREB, Ca^{2+}/cAMP-response element-binding protein; CLICKs, CaMK-like CREB kinases; VMH, ventromedial hypothalamus; HMG-CoA, 3-hydroxy-3-methylglutaryl-coenzyme A; RACE, rapid amplification of cDNA ends; HA, hemagglutinin; GFP, green fluorescent protein; EGFP, enhanced GFP; wt, wild type; PBS, phosphate-buffered saline; MBP, myelin basic protein; HBSS, Hanks' balanced salt solution; CNS, central nervous system; CeA, central nucleus of amygdala; CMV, cytomegalovirus.

geting of various signaling molecules to cellular membrane compartments (22, 23). CLICK-III was identified during a screen for novel putative CaMK-like CREB kinases (CLICKs), as a kinase homologous to CLICK-I and CLICK-II (the cloning and characterization of CLICK-I and -II will be described elsewhere).[2]

The kinase activity of CLICK-III was similar in many respects to CaMKIα and related kinases. Thus, full activation of CLICK-III required both Ca^{2+}/CaM and phosphorylation by a CaMKK (24–31). In addition, Ca^{2+}/cAMP-response element-binding protein (CREB) (4, 32) was a good substrate for CLICK-III, at least *in vitro*. Interestingly, CLICK-III transcripts were most abundant in neurons, with the highest levels in limited nuclei such as the central nucleus of the amygdala (CeA) and the ventromedial hypothalamus (VMH). Furthermore, CLICK-III was found to be anchored to membrane compartments, consistent with the presence of the *CAAX* motif at its C-terminal end. A point mutation in the *CAAX* motif and treatment with compactin, a 3-hydroxy-3-methylglutaryl coenzyme A (HMG-CoA) reductase inhibitor (33), disrupted such membrane localization, suggesting that membrane localization of CLICK-III occurred in a prenylation-dependent way. These findings provide a novel mechanism by which neuronal CaMK activity could be targeted to specific membrane compartments.

EXPERIMENTAL PROCEDURES

Cloning and Plasmid Constructions—Human hippocampal cDNA was prepared from poly(A)$^+$ RNA (Clontech) using Omniscript reverse transcriptase (Qiagen) and oligo(dT) primers. An hCLICK-III cDNA was obtained by nested PCR using two primer pairs (F1, 5′-CCA CTC CCT GCA ATA AAG CAT CCT C-3′, and R1, 5′-CTG CCT ATG AGT GGG AGA GGC CTT T-3′ as a first primer set; F2, 5′-TGG AGG CAA TGG GTC GAA AGG AAG AA-3′, and R2, 5′-TGT CCA TTT CTT TCA GTC CTG TTG A-3′ as a nested primer set) and subcloned into pCR-Blunt vector (Invitrogen). ICR mouse hippocampal poly(A)$^+$ RNA was purified using Trizol (Invitrogen) and μMACS mRNA isolation kit (Miltenyl Biotec), and mCLICK-III was subsequently obtained by the 3′-RACE procedure, using SMART RACE cDNA amplification kit (Clontech) following the manufacturer's instructions. A gene-specific 5′-primer for 3′-RACE was designed based on the cDNA sequence of hCLICK-III and that of rat CaMKIγ (19) at the 5′-untranslated region adjacent to the first methionine (5′-GCA GCT TCA ACT CTG GAG G-3′). A single RACE-amplified fragment was obtained and subcloned into pCR-Blunt vector, and its nucleotide sequence was determined. Two independent clones were recovered and yielded an identical sequence. To construct pIRES-HAmCL3wt and pIRES-HAmCL3dC, cDNA fragments were amplified by PCR using primers F and R1 or R2 (F, 5′-GGG GGA ATT CTG GCG GCC GCT ATG GGG CGT AAG GAG GAG GAG-3′, and R1 for wt, 5′-GGG GGA ATT CGT TTG GCG GCC GCC TCC TGG GAT CAC ATA ACG AG-3′, or R2 for dC, 5′-GGG GGA ATT CGT TTG GCG GCC GCA AAG TTC TTC TAA ATC TGG AG-3′) and inserted in-frame downstream to an HA tag cassette at the *Not*I site of pIRES-S-Tag-EGFP vector (a kind gift from Dr. Hirohide Takebayashi). To construct pcDNA3-HAmCL3wt and pcDNA3-HAmCL3dC, *Eco*RV/*Eco*RI fragments of each pIRES-S-Tag-EGFP construct were blunted and subcloned into the *Eco*RV site of pcDNA3 (Invitrogen). To construct pEGFP-mCL3 and pEGFP-mCL3C474S, cDNA fragments amplified with primers F and R1 or R2 (F, 5′-GCT TCG AAT TCA GGC TTC AAC TC-3′, and R1 for wt, 5′-CCC TCC CGC GGT CAC ATA ACG AGA GAC ACC CCA GTC-3′, or R2 for C474S, 5′-CCC TCC CGC GGT CAC ATA ACG AGA CAC ACC CCA GTC-3′) were inserted into a pEGFP-C3 vector (Clontech) cut at *Eco*RI and *Sac*II sites. To construct pEGFP-CLVM, two oligonucleotide pairs (5′-CTG TCT CGT TAT GTG AGT GCA CA-3′ and 5′-GAT CTG TGC ACT CAC ATA ACG AGA CAG GGC C-3′) were annealed, phosphorylated, and inserted to a pEGFP-C2 vector (Clontech) at the *Apa*I and *Bam*HI sites. To construct pd2EGFPN1-CaMKKactiveMyc, a 1.3-kb cDNA fragment encoding the N-terminal kinase domain of rat CaMKKα was PCR-cloned from a Sprague-Dawley rat hippocampal cDNA pool, fused to a Myc epitope tag using a pair of primers (F, 5′-ACG GTA CCA TGG AGC GCA GTC CAG CCG, and R, 5′-ATT GGA TCC CTA CAG GTC CTC CTC GCT GAT CAG CTT CTG CTC TCC ATG CTT GGT CAC CCA-3′), and inserted into a pd2EGFPN1 vector (Clontech) cut at *Kpn*I and *Bam*HI site. To construct pEGFP-rCaMKIα, a cDNA fragment corresponding to the full-length coding region of rat CaMKIα was obtained by PCR using primers (F, 5′-AAC TCGAGT GGG CCA TGC CAG GGG CAG TG-3′, and R, 5′-ATT GGA TCC TAG TCC TAG TCC ATG GCC CTA GAG CT-3′), subcloned into a pBluescriptII KS(+) vector cut at *Xho*I and *Bam*HI sites, and thereafter transferred in-frame to pEGFP-C1 vector (Clontech) at *Eco*RI and *Bam*HI sites. All inserts in the expression vectors were verified by sequencing.

Northern Blotting—For Northern blot analysis, a total RNA blot filter was purchased from Seegene (Mouse Brain Aging Blot), and poly(A)$^+$ RNA blot filters were from Clontech (all other blots). Double-stranded probe templates, corresponding to the unique sequence of CLICK-III at the C-terminal region, were generated by PCR using primers (F, 5′-AAG CCT CAG AAA CCT CTA GAC CCA G-3′, and R, 5′-TTC AGA CCC AAG CTG GGG CTC CAT CT-3′ for hCLICK-III; F, 5′-ATG AAC CTG CAC AGC CCC AGT G-3′, and R, 5′-TTA TTG GCC TTT CTG AAG AGG-3′ for mCLICK-III). The probes were labeled with [α-^{32}P]dCTP using Ready-to-Go DNA labeling beads (Amersham Biosciences) and hybridized with the filters in ExpressHyb Hybridization Solution (Clontech) at 68 °C. The filters were washed four times in 0.05% SDS, 2× SSC for 10 min at 50 °C, washed once in 0.1% SDS, 0.1× SSC for 40 min at 50 °C, and subjected to x-ray film autoradiography.

In Situ Hybridization—Brain cryosections (10 μm) were obtained from 2-month-old female ICR mice and processed for *in situ* hybridization as described previously (34). N-terminal (231 bp) and C-terminal (374 bp) fragments were amplified by PCR (5′-GCA GCT TCA ACT CTG GAG G-3′ and 5′-TAG GCT GCT GTC CCG GAA GG-3′ for N-terminal fragment, 5′-ATG AAC CTG CAC AGC CCC AGT G-3′ and 5′-TTA TTG GCC TTT CTG AAG AGG-3′ for C-terminal fragment) and subcloned into pBluescriptII KS(+) vector at the *Sac*II site. [^{35}S]-Labeled riboprobes were generated using T7 RNA polymerase (Stratagene) and [α-^{35}S]CTP.

CaM-Sepharose Binding Assay—COS-7 cells were maintained in Dulbecco's modified Eagle medium containing 10% fetal calf serum. Cells were subcultured in 6-cm dishes 12 h before transfection. pcDNA3-HAmCL3wt (2 μg) or empty vector (2 μg) were transfected using 4 μl of LipofectAMINE 2000 reagent (Invitrogen). After 24 h, the cells were washed twice with ice-cold PBS(−) and lysed in lysis buffer containing 50 mM Tris-HCl (pH 8.0), 150 mM NaCl, 2 mM $CaCl_2$, 1% Triton X-100, 0.5% deoxycholate, and protease inhibitors (Complete tablet, Roche Applied Science). After the protein concentrations were determined using a DC protein assay kit (Bio-Rad), 250 μg of the lysates were incubated with 15 μl of CaM-Sepharose (Amersham Bioscience) in the lysis buffer for 2 h at 4 °C. Beads were washed for six times in the lysis buffer or Ca^{2+}-free lysis buffer containing 50 mM Tris-HCl (pH 8.0), 150 mM NaCl, 2 mM EGTA, 1% Triton X-100, 0.5% deoxycholate, and protease inhibitors. CaM-bound mCLICK-III was detected by Western blot with an anti-HA tag monoclonal antibody (1:2500, 12CA5; Roche Diagnostics).

Immunoprecipitate Kinase Assay—COS-7 cells were plated onto 6-well plates at a density of 2 × 10^5 per well, and 12 h later were transiently transfected with pcDNA3-HAmCL3wt (0.3 μg), pcDNA3-HAmCL3dC (0.3 μg), or empty vector (0.3 μg) and pd2EGFPN1-CaMKKactiveMyc (0.6 μg), or empty vector (0.6 μg) using LipofectAMINE 2000 reagent. For immunoprecipitate kinase assay, cells were washed twice with ice-cold PBS(−) and lysed in lysis buffer containing 20 mM Tris-HCl (pH 8.0), 100 mM NaCl, 5 mM $MgCl_2$, 1% Nonidet P-40, 1 mM dithiothreitol, 25 mM NaF, 10 mM β-glycerophosphate, 5 mM sodium pyrophosphate, 0.1 μM calyculin A, and protease inhibitors. Lysates were immunoprecipitated with an anti-HA antibody (12CA5) and protein-G-Sepharose (Amersham Biosciences). Immunoprecipitates were washed three times in the lysis buffer and washed twice in kinase buffer containing 50 mM HEPES-NaOH (pH 7.5), 10 mM $MgCl_2$, 1 mM Ca^{2+}, 20 mM β-glycerophosphate, 0.02% Nonidet P-40, 1 mM dithiothreitol, and protease inhibitors. Kinase assay was performed in the presence of 1 μM CaM, 50 μM ATP, 0.5 μCi of [γ-^{32}P]ATP in the kinase buffer using 2.5 μg of CREM (cAMP-response element modulator) (Santa Cruz Biotechnology) or 5 μg of MBP (Calbiochem) as substrates for 10 min at 30 °C. For kinase assay without Ca^{2+}/CaM, 1 μM CaM was omitted, and 1 mM EGTA was substituted for 1 mM Ca^{2+} in the kinase buffer.

Luciferase Assay—COS-7 cells were plated onto 24-well plates at a density of 5 × 10^4 per well, and 12 h later were transfected with pFR-Luc, pFA-CREB, pRL-CMV (200 ng, 50 ng, 4 ng each; Stratagene), and pIRES-HAmCL3dC (100 ng). 24 h after transfection, luciferase

[2] S. Ohmae, S. Takemoto-Kimura, and H. Bito, manuscript in preparation.

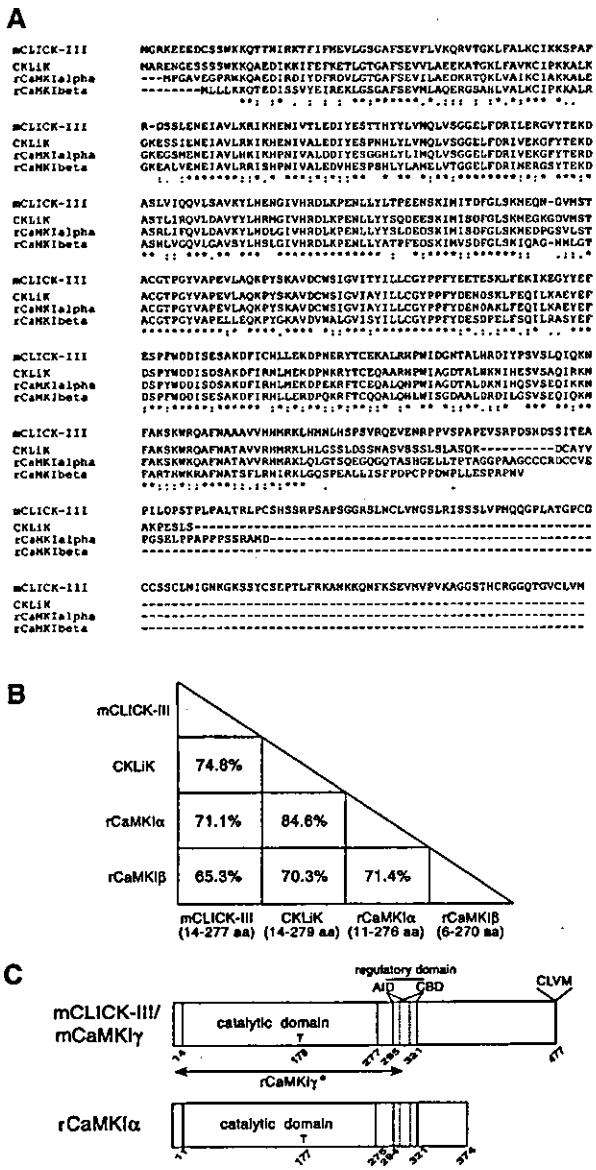

FIG. 1. **CLICK-III/CaMKIγ is an isoform of the CaMKI family with an unusually extended C-terminal domain.** *A*, the deduced amino acid sequence of mCLICK-III was aligned with CKLiK, rCaMKIα, and rCaMKIβ by using the ClustalW Multiple Sequence Alignment Program version 1.8. The *asterisks* indicate positions of identical amino acid residues. The *colons* and *dots* indicate stronger and weaker degrees of residue conservation, respectively. *B*, comparison of amino acid identities between kinase domain sequences of known CaMKI-related kinases. The kinase domain of mCLICK-III shows high identity with all known CaMKI-related kinases, CKLiK (74.8%), CaMKIα (71.1%), and rCaMKIβ (65.3%), respectively, in the order of identity (*left column*). The exact position of amino acid (*aa*) residues used for comparison are shown in *parentheses*. *C*, similarity and difference between CLICK-III and other CaMKI-related kinases. CLICK-III shares a high homology in its catalytic domain at the N terminus followed by a regulatory domain consisting of an autoinhibitory domain (*AID*) and a Ca^{2+}/CaM binding domain (*CBD*). Unlike the other CaMKI-related kinases, however, mCLICK-III has a distinctively longer C-terminal region ending with a putative *CAAX* motif (*CLVM*). A 309-amino acid-long partial sequence of rat of CLICK-III has been reported before as a rat CaMKIγ (*asterisk*) (19). GenBank™ accession numbers are as follows: mCLICK-III, AY212936; CKLiK, AF286366; rCaMKIα, L24907 and L26288; rCaMKIβ, D86556; and rCaMKIγ (partial cDNA), D86557.

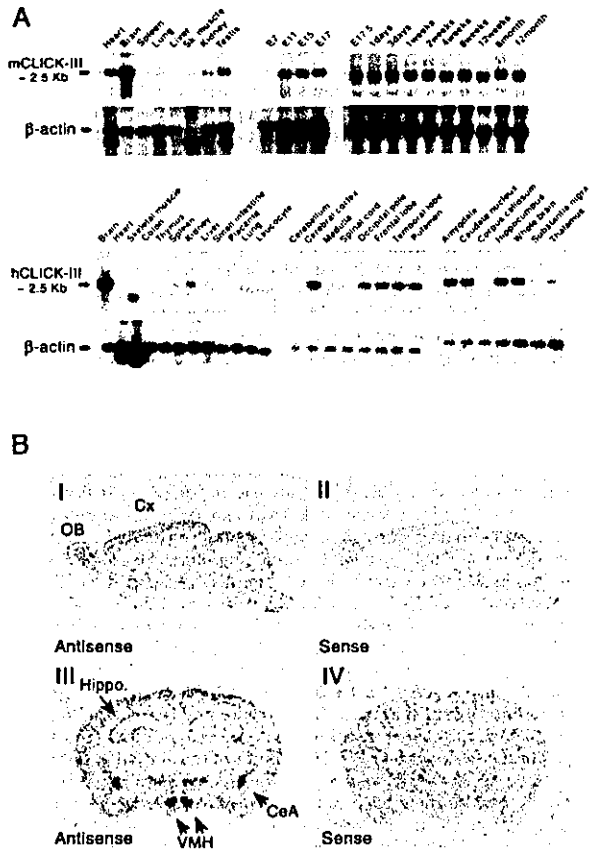

FIG. 2. **Abundant expression of CLICK-III transcripts in the CNS.** *A*, Northern blotting using specific probes for CLICK-III showed that both mCLICK-III and hCLICK-III are most strongly expressed in the brain. Note that mCLICK-III transcripts are expressed from embryonic day (*E*) 11, and hCLICK-III transcripts are expressed in a forebrain-specific manner in the CNS. *Sk*, skeletal. *B*, *in situ* hybridization was performed with ^{35}S-labeled riboprobes. Film autoradiographs of mouse brain parasagittal (*I* and *II*) and coronal sections (*III* and *IV*) showed specific hybridization signals for mCLICK-III antisense probes in restricted brain areas such as the olfactory bulbs (*OB*), the cerebral cortex (*Cx*), the hippocampus (*Hippo.*), the central nucleus of amygdala (*CeA*), and the ventromedial nucleus of hypothalamus (*VMH*). These signals disappeared when sense probes were used (*II* and *IV*).

activity was measured using Dual-Luciferase Reporter Assay System (Promega) according to the manufacturer's protocol. The firefly and the *Renilla* luciferase activities were both measured using SIRIUS luminometer (Berthold). All results were normalized using *Renilla* luciferase (pRL-CMV), which was co-transfected with the other reporter genes (pFR-Luc and pFA-CREB).

Culture and Transient Transfection of CA1/CA3 Hippocampal Neurons—Culture of mouse CA1/CA3 hippocampal neurons was carried out as described previously for rat (16). A cDNA transfection was carried out at 7 days *in vitro* using a modification of the calcium phosphate method.[3]

BODIPY-TR-ceramide Labeling and Fluorescence Microscopy—For BODIPY-TR-ceramide (Molecular Probes) and green fluorescent protein (GFP) imaging, COS-7 were plated on Lab-Tek chambered coverglass (4 well, Nunc) and transfected with expression vectors (0.4 μg/well), pEGFP-rCaMKIα, pEGFP-mCL3, pEGFP-mCL3C474S, and pEGFP-CLVM using LipofectAMINE 2000 reagent. After 24 h, the cells were rinsed twice in HBSS/HEPES, incubated for 20 min at room temperature with 2.5 μM BODIPY-TR ceramide/bovine serum albumin in HBSS/HEPES. The cells were washed twice with HBSS/HEPES and replaced with pre-warmed fresh medium, followed by a 1-h incubation

[3] S. Takemoto-Kimura and H. Bito, manuscript in preparation.

in a CO_2 incubator. To simultaneously acquire GFP and BODIPY-TR-ceramide images under live conditions, a Carl Zeiss LSM 510 system equipped with a Carl Zeiss Axiovert 100TV inverted microscope and a ×63 Plan-Apochromat (NA 1.4, oil) objective (Carl Zeiss) was used. For all images, stacks of multiple Z-scan sections were obtained, and projected images were calculated off-line using a projection software on the LSM 510 system. All pseudocolor representations were assembled using Photoshop version 5.5 (Adobe). For compactin pretreatment, the normal medium was replaced with a growth medium containing 40 μM compactin (Wako Pure Chemicals) for 12 h. No apparent phototoxicity was observed under our experimental conditions.

Subcellular Fractionation—COS-7 cells were grown to 70% confluency on a 10 cm-dish and transfected with each expression vector (4 μg per dish) using LipofectAMINE 2000 reagent. 48 h after transfection, the cells were washed twice in ice-cold PBS(−), suspended in 250 μl (per dish) of homogenizing buffer containing 10 mM HEPES-NaOH (pH 7.5), 10 mM KCl, 2 mM $MgCl_2$, protease inhibitors, disrupted in a Potter-Elvehjem homogenizer with 40 strokes, and adjusted to 0.25 M sucrose. To remove unbroken cells and nuclei, the homogenate was centrifuged at 600 × *g* for 10 min. The supernatant was separated by centrifugation at 100,000 × *g* for 60 min. After collecting the resulting supernatant (cytosolic fraction, S), the membrane pellet was washed once in the homogenizing buffer containing 0.25 M sucrose and again centrifuged at 100,000 × *g* for 60 min. For the salt wash experiment, the 600 × *g* supernatant was divided into two microtubes and separated by ultracentrifugation at 100,000 × *g* for 60 min. The membrane pellet was resuspended in homogenization buffer containing 10 mM HEPES-NaOH (pH 7.5), 10 mM KCl, 2 mM $MgCl_2$, 0.25 M sucrose or high salt homogenization buffer containing 1 M NaCl, followed by incubation on ice for 1 h, and ultracentrifuged again at 100,000 × *g*. For all analyses, the membrane pellets were finally extracted with the elution buffer containing 25 mM HEPES-NaOH (pH 7.5), 2% SDS, 150 mM NaCl, protease inhibitors for 1 h at room temperature and centrifuged for 15 min at 15,000 rpm. This supernatant was collected and designated as crude membrane fraction (P or P'). The volume of the elution buffer was adjusted to be equal to the volume of input (identical to the 600 × *g* supernatant). For Western blot analyses, one-third volume of 4× Laemmli buffer was added and boiled for 4 min, and 20 μl of each fractions were subjected to SDS-PAGE. For compactin treatment, the medium was replaced with growth medium containing 40 μM compactin for 16 h.

Western Blot Analysis—After SDS-PAGE, the proteins were transferred onto a nitrocellulose membrane (Optitran BAS-85, Schleicher & Schuell), and immunoreactive proteins were detected using ECL-Plus (Amersham Biosciences) with the following concentration of primary antibodies: anti-HA tag monoclonal antibody (1:2500, 12CA5; Roche Applied Science), anti-GFP monoclonal antibody (1:1000, 3E6; Molecular Probes), and anti-phospho-CREB (Ser-133) polyclonal antibody (1:1000; Cell Signaling). Horseradish peroxidase-linked anti-mouse or anti-rabbit IgG (1:2000; Amersham Biosciences) were used as secondary antibodies. The chemiluminescence image was acquired using a FAS-1000 system (Toyobo) equipped with a 16-bit cooled CCD camera. For quantification of signal intensity of detected immunoreactive bands, a rectangular window, which had a sufficient area to completely surround each band, was defined, and the total pixel intensity of each area was calculated using Photoshop 6.0 (Adobe). The signal intensity was normalized as a percentage of the total intensity, calculated as the sum of the band intensities detected in cytosolic and membrane fractions (S or P or P'/(S + P)). Statistical analyses were carried out using Prism 3.0 (GraphPad software). Statistical significance ($p < 0.05$) was determined between two groups using unpaired Student's *t* test and between three groups using one-way analysis of variance (followed by post hoc Bonferroni and Neuman-Keuls tests). All data are given as means ± S.E.

RESULTS

Molecular Cloning of CLICK-III, a Novel Brain-enriched CaMK—During the course of studying two novel putative CaMK-like CREB kinase-I and -II (CLICK-I and -II) cloned by degenerate PCR strategies,[2] BLAST search revealed the presence of a putative human gene product with high homology to both CLICKs. We named this novel kinase human CLICK-III. A putative open reading frame of human CLICK-III had been deposited as a novel rat Ca^{2+}/calmodulin-dependent protein kinase-like gene, an assembly of presumed exon sequences obtained from the draft Human Genome Sequence (GenBank™ accession number AL023754). We cloned a human CLICK-III (hCLICK-III) cDNA (GenBank™ accession number AY212935) by PCR from a human hippocampal cDNA pool, using primer sequences corresponding to the deposited sequence, and we confirmed the authenticity of this gene product. We next used a 3'-RACE strategy to obtain a full-length mouse hippocampal CLICK-III cDNA (GenBank™ accession number AY212936). Mouse CLICK-III (mCLICK-III) showed a high degree of amino acid identities with CKLiK, a recently reported CaMK-like kinase (18), as well as with rat CaMKIα (13) and CaMKIβ (19) (Fig. 1, *A* and *B*). A partial sequence of a rat ortholog of CLICK-III was previously reported as rCaMKIγ (19) (*asterisk*, Fig. 1*C*).

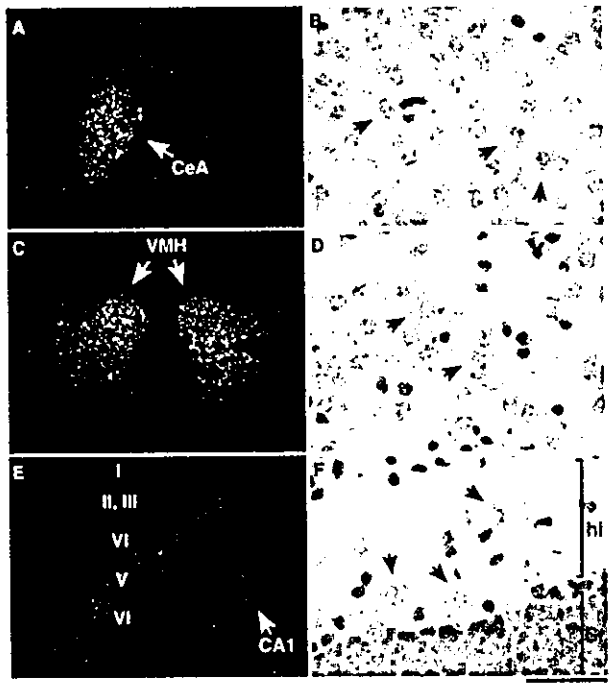

FIG. 3. **CLICK-III transcripts are expressed in neurons.** Dark- (*A*, *C*, and *E*) and bright-field (*B*, *D*, and *F*) photomicrographs showed strong signals in the central nucleus of amygdala (*A*, *CeA*) and the ventromedial hypothalamic nucleus (*C*, *VMH*) (also see Fig. 2*B*, *III*). Silver grains were present only on neuronal cell bodies (*arrows*, *B* and *D*). Moderate signals were detected on the layer *V* pyramidal neurons in the cerebral cortex and the *CA1* pyramidal neurons in the hippocampus (*E*). In the hippocampus, non-principal neurons were also labeled with silver grains (*arrows*, *F*). *CA1*, CA1 area for Ammon's horn; *hi*, the hilus of the dentate gyrus; *Gr*, the granule cell layer of the dentate gyrus. *Scale bars*, *A*, *C*, and *E*, 0.5 mm; *B*, *D*, and *F*, 50 μm.

The open reading frame of CLICK-III cDNAs contained an N-terminal kinase domain, a conserved threonine at position 178 in the activation loop, and an overlapping autoinhibitory/Ca^{2+}/CaM-binding domain in its middle portion; these domains showed high homology across the CaMKI-related kinases (Fig. 1*B*). The C-terminal end of CLICK-III was unusually extended in comparison with CKLiK, CaMKIα, and CaMKIβ, suggesting a unique role for CLICK-III (Fig. 1*C*). The very C-terminal end of hCLICK-III and mCLICK-III were, however, divergent, indicating the existence of multiple C-terminal variants (data not shown).

As shown in Fig. 2*A*, Northern blot analyses suggested that in adult tissues, mCLICK-III was highly expressed in the brain, although heart, testis, and kidney also showed detectable amounts of hybridization signals. The mCLICK-III transcript first became detected at embryonic day 11 (E11), in parallel with the onset of the development of the central nervous system (CNS). Its expression level remained constant from E11 onward, throughout development and during adulthood

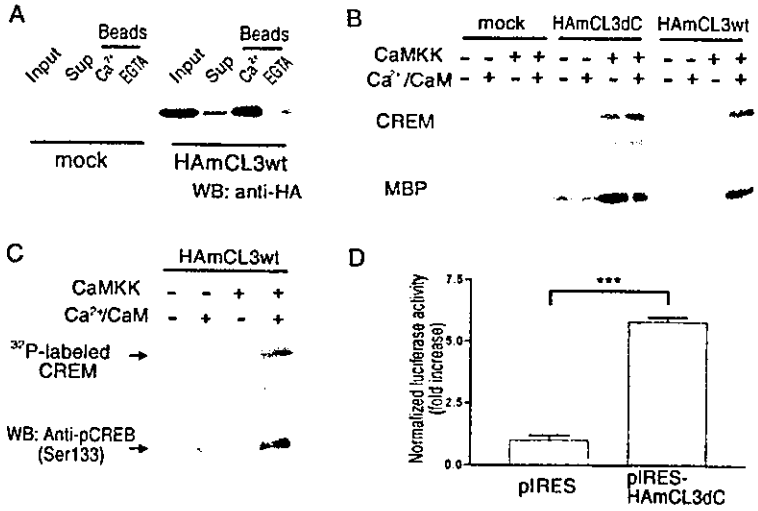

FIG. 4. **Activation of CLICK-III by Ca^{2+}/CaM and CaMKK.** *A*, mCLICK-III expressed in COS-7 cells is bound to CaM-Sepharose beads in the presence of Ca^{2+}. Lysates from COS-7 cells transfected with either an empty vector (*mock*) or a mCLICK-III cDNA (*HAmCL3wt*) were incubated with CaM-Sepharose beads. mCLICK-III remained bound to CaM-Sepharose after washing in the presence of 2 mM Ca^{2+} (*Beads, Ca^{2+}*), whereas most CLICK-III was washed out in 0 mM Ca^{2+}, 2 mM EGTA (*Beads, EGTA*). *WB*, Western blot. *B*, immunoprecipitate kinase assays of CLICK-III. COS-7 cells were transfected with an empty vector (*mock*), a wild type mCLICK-III cDNA (*HAmCL3wt*), or mCLICK-III C-terminal deletion mutant (*HAmCL3dC*) with (+) or without (−) a cDNA encoding a constitutive active form of rat CaMKKα (*CaMKK*). After immunoprecipitation with an anti-HA antibody, kinase assays were performed in the presence (+) or the absence (−) of Ca^{2+}/CaM using MBP (5 μg) or CREM (2.5 μg) as substrates. Note that both mCL3wt and mCL3dC require CaMKK activity for their full activation. C-terminal deletion mutant of mCLICK-III showed a clear constitutive kinase activity in the presence of CaMKK, independent of the presence of Ca^{2+}/CaM, whereas the wild type kinase was only active in the presence of Ca^{2+}/CaM. *C*, CREM phosphorylation was also detected in a manner similar to ^{32}P incorporation, using an anti-phospho-CREB (Ser-133) antibody. *D*, the C-terminal deletion mutant of CLICK-III can activate CREB-dependent transcription in COS-7. Cells were transfected with CLICK-III C-terminal deletion mutant (*pIRES-HAmCL3dC*) and reporter genes coding Gal4-CREB and UAS-luciferase and collected, and lysates were extracted to measure the luciferase activity 24 h later. The *bars* represent luciferase activities relative to that of mock-transfected lysates (*pIRES*) and are shown as means ± S.E. (n = 3). *** denotes $p < 0.001$.

(Fig. 2*A*, *upper panels*). In human mRNA blots, CLICK-III expression was almost confined to the brain, with small amount of signals in the skeletal muscles, kidney, spleen, and liver (Fig. 2*A*, *lower panels*). Within the CNS, the strongest signal was detected in the forebrain neocortex (cerebral cortex, occipital pole, frontal lobe, and temporal lobe), the striatum (putamen and caudate nucleus), and the limbic system (amygdala and hippocampus) (Fig. 2*A*, *lower panels*).

CLICK-III Is Neuronally Expressed and Is Abundant in the CeA and the VMH—We next examined CNS expression of CLICK-III mRNA by *in situ* hybridization using ^{35}S-labeled cRNA riboprobes. X-ray film autoradiography of hybridized parasagittal and coronal sections showed specific signals in the neuronal cell layers of the cerebral cortex, olfactory bulb, and hippocampus (Fig. 2*B*, *I* and *III*). Most remarkably, intense hybridization signals were shown in the CeA and the VMH (Fig. 2*B*, *III*). We obtained identical results using two independent antisense probes, either from the N-terminal or from C-terminal regions (data not shown), whereas sense probes only generated background signals (Fig. 2*B*, *II* and *IV*). Hybridization in the presence of excess cold riboprobes also completely abolished the antisense probe signals (data not shown), confirming the specificity of these obtained signals.

Emulsion autoradiography of individual sections revealed that CLICK-III was particularly expressed in neurons, but not found in glia, in any areas that we examined. Heavy amounts of silver grains associated with most neuronal cell bodies present in the CeA (Fig. 3, *A* and *B*) and the VMH (Fig. 3, *C* and *D*). Pyramidal cells in the cerebral cortex, especially in the layer V, and those in the area CA1 of the hippocampus were also positive in CLICK-III mRNA signals (Fig. 3*E*). In contrast, in the dentate gyrus of the hippocampus, only scattered non-principal cells, presumably hilar interneurons, had significant amount of silver grains (Fig. 3*F*).

Taken together, these sets of data established that CLICK-III was a CaMKI family member specifically expressed in neurons, with a remarkable abundance in the CeA and VMH. Such specificity in its expression profile particularly stands out

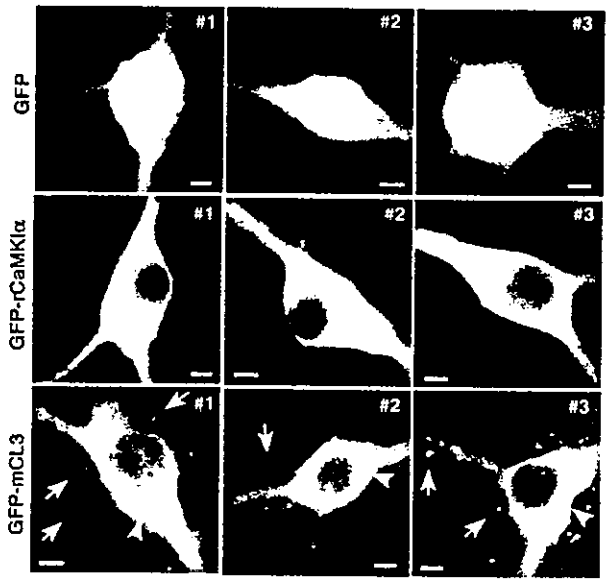

FIG. 5. **GFP-rCaMKIα and GFP-mCL3 show distinct subcellular localization in hippocampal neurons.** Mouse CA1/CA3 hippocampal neurons were transfected with GFP, GFP-rCaMKIα, and GFP-mCL3 for 7 days *in vitro*, fixed 48 h later, and examined by confocal microscopy. Three representative neurons were shown for each construct (*#1–#3*). GFP showed diffuse distribution across the cell, whereas GFP-rCaMKIα was diffusely expressed mainly in the cytoplasm. In contrast, GFP-mCL3 expression was more localized in specific intracellular compartments (*arrowheads*) and concentrated at the tips of filopodia-like processes (*arrows*). *Bar*, 5 μm.

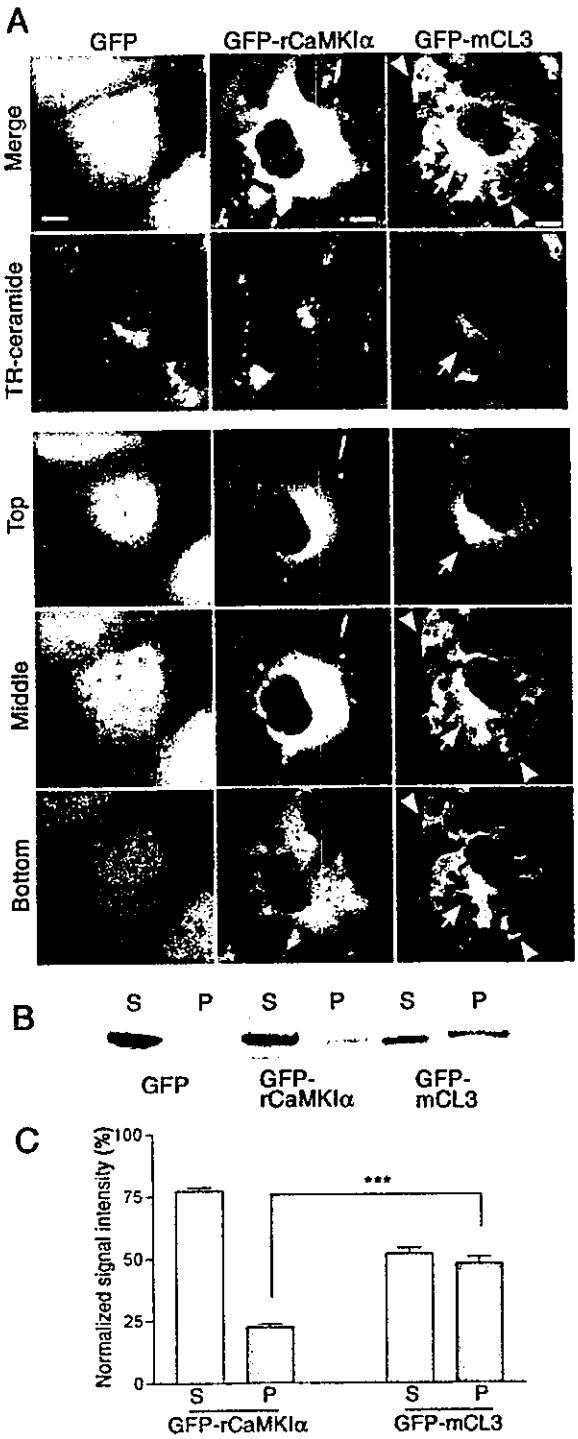

FIG. 6. **Localization of GFP-mCL3 with the Golgi complex and plasma membranes in COS-7 cells.** *A*, COS-7 cells transfected with GFP, GFP-rCaMKIα, and GFP-mCL3 were stained with a Golgi-specific vital dye (BODIPY TR-ceramide) and examined under live conditions. Projected images from stacks of z-planes (*Merge* and *TR-ceramide*) and single z-plane images taken near the *bottom*, *middle*, and *top* of the cells showed localization of CLICK-III to the Golgi complex (*arrows*) and to the plasma membranes (*arrowheads*). *Green*, GFP image; *red*, BODIPY TR-ceramide. *Bar*, 10 μm. *B*, lysates of COS-7 cells transfected with the indicated constructs were fractionated by ultracentrifugation at 100,000 × *g*. The supernatants (*S*) were collected as cytosolic fractions, and the pellets (*P*) were washed once and centrifuged again. The resulting pellet was recovered as crude membrane fraction (*P*). Each fraction was blotted and visualized using an anti-GFP antibody. *C*, chemiluminescent signal intensities, quantified by a CCD camera-based imaging system, were presented in percentages relative to the total signal intensities detected in both fractions (*S* + *P*). The *bars* represent means ± S.E. ($n = 4$). ***, $p < 0.001$.

TABLE I
C-terminal sequences of Ras proteins and mCLICK-III
CAAX motifs are shaded with a gray box.

mCLICK-III	GSTHCRGGQTGVCL**CVM**
H-ras	PDESGPGCMSCKCVLS
N-ras	SDDGTQGCMGLPCVVM
K-ras(4B)	DGKKKKKKSKTKCVIM

among all CaMKs presently identified (16–21, 35–37).

Enzymatic Properties of CLICK-III—We next tested whether CLICK-III was indeed a Ca^{2+}/CaM-dependent protein kinase, as suggested from its domain structure (Fig. 1*B*). To this end, an HA-tagged CLICK-III was constructed and transfected to COS-7 cells. Crude lysates of transfected COS-7 cells were collected and incubated with CaM-Sepharose beads in the presence of 2 mM Ca^{2+}. The beads were centrifuged and separated from the supernatant and then washed several times in the presence or absence of Ca^{2+}. SDS-PAGE analyses showed that HA-immunoreactive bands were mostly recovered with the beads in the presence of Ca^{2+}, whereas they were largely washed out in 0 Ca^{2+}, 2 EGTA (Fig. 4*A*). Thus, CLICK-III was clearly able to bind CaM in a Ca^{2+}-dependent manner.

Ca^{2+}/CaM-dependent regulation of the protein kinase activity of CLICK-III was investigated using an immunoprecipitate kinase assay, with MBP and CREM as kinase substrates (Fig. 4*B*). Both Ca^{2+}/CaM and CaMKK cotransfection were required to reach maximal levels of activation of the wild type CLICK-III (HAmCL3wt). In contrast, a C-terminal deletion mutant in which the entire autoinhibitory/Ca^{2+}/CaM binding domain was removed (HAmCL3dC) showed a constitutive, Ca^{2+}-independent kinase activity even in the absence of Ca^{2+}, when active CaMKK was cotransfected (Fig. 4*B*). CLICK-III activity monitored with [γ-^{32}P]ATP incorporation into CREM closely paralleled the amount of phospho-CREB Ser-133 immunoreactivity, suggesting that wild type CLICK-III is able to directly phosphorylate CREB at Ser-133, in a Ca^{2+}/CaM- and CaMKK-dependent manner, at least *in vitro* (Fig. 4*C*). We further confirmed that CLICK-III may work as CREB kinase *in vivo* by using a Gal4-CREB/UAS-luciferase reporter system. Transfection of a constitutively active CLICK-III (pIRES-HAmCL3dC) significantly augmented CREB-dependent gene expression in COS-7 cells (Fig. 4*D*). The result was normalized using *Renilla* luciferase (pRL-CMV), which was co-transfected with the other reporter genes (pFR-Luc and pFA-CREB).

Taken together, these data indicated that the enzymatic properties of CLICK-III recapitulated all major features of CaMKI isoforms, such as dual regulation by Ca^{2+}/CaM and CaMKK, and activation of CREB pathway *in vitro* and in a heterologous system.

Membrane Localization of CLICK-III in Hippocampal Neurons and in COS-7 Cells—As we failed to raise high titer antibodies against CLICK-III, we expressed GFP-tagged CLICK-III in hippocampal pyramidal neurons 7 days *in vitro*, and we monitored its subcellular distribution in fixed (Fig. 5) or live samples (data not shown). Under either condition, GFP alone was diffusely distributed throughout the cytoplasm and the nucleus, whereas GFP-rCaMKIα remained largely ex-

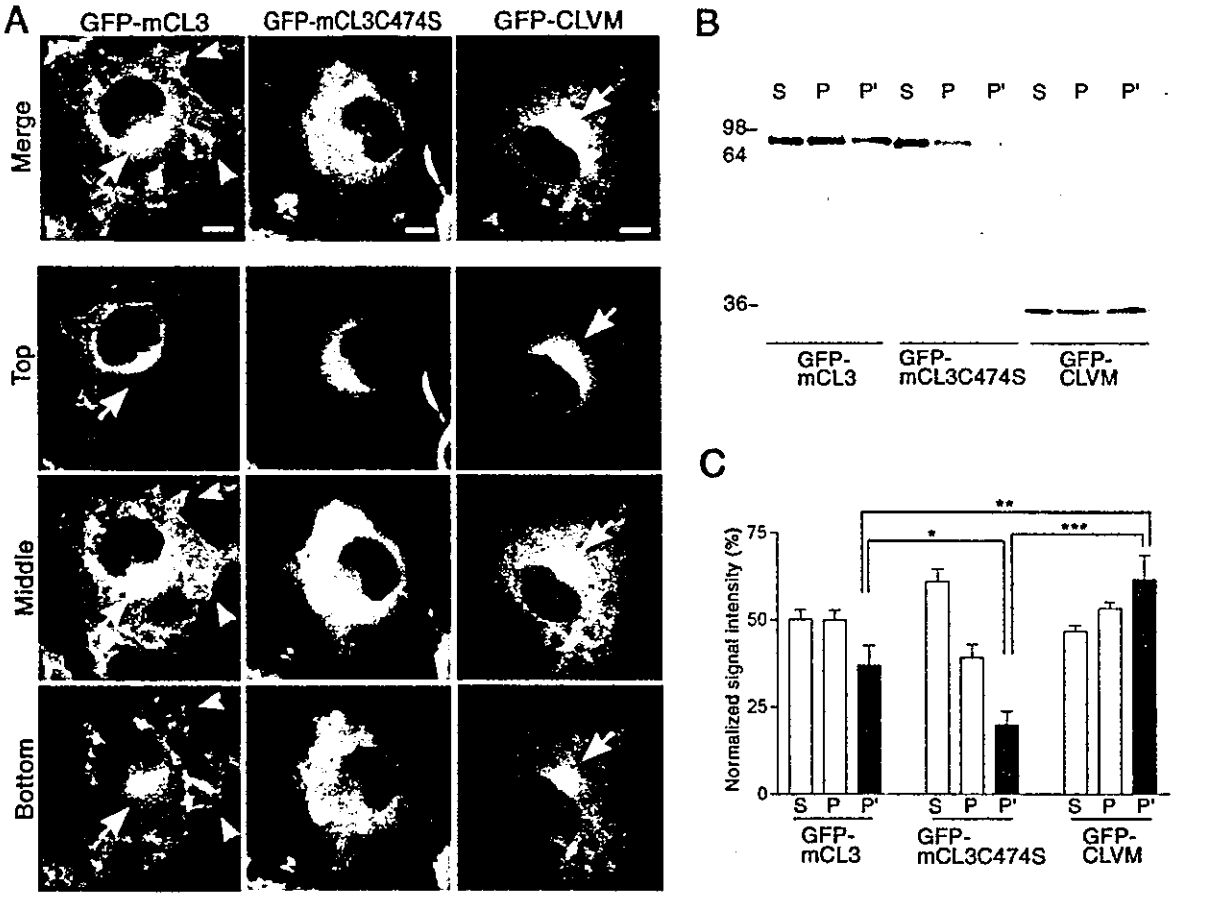

FIG. 7. **A critical role of the C-terminal *CAAX* motif in determining mCLICK-III localization.** *A*, COS-7 cells transfected with either wild type CLICK-III (*GFP-mCL3*), a mutant that has a point mutation at the prenylation site of *CAAX* motif (*GFP-mCL3C474S*), or *GFP-CLVM* were stained with BODIPY TR-ceramide and examined alive. The *arrows* and *arrowheads* indicate the localization to the Golgi complex and to the plasma membranes, respectively. *Merge*, projected images; *top*, *middle*, and *bottom*, single z-plane images. *Green*, GFP image; *red*, BODIPY TR-ceramide. *Bar*, 10 μm. *B*, COS-7 lysates were fractionated by ultracentrifugation at 100,000 × *g*. The supernatants were collected (*S*), and the pellets (*P*) were washed in either normal homogenization buffer or high salt homogenization buffer, followed by ultracentrifugation at 100,000 × *g*. The cytosolic fractions (*S*), the membrane fractions (*P*), and the high salt-washed membrane fractions (*P'*) were subjected to Western blotting with an anti-GFP antibody. *C*, quantification of signal intensities detected in *B*. The *bars* represent means ± S.E. (wt, $n = 4$; C474S, $n = 4$; CLVM, $n = 3$). *, $p < 0.05$; **, $p < 0.01$; ***, $p < 0.001$.

cluded from the nucleus, in keeping with prior reports (Fig. 5) (15, 16). A striking difference was noted in the subcellular localization of GFP-tagged CLICK-III (GFP-mCL3); GFP-mCL3 distribution was not diffuse but seemed rather associated with intracellular compartments reminiscent of endomembrane systems such as the Golgi complexes or the endoplasmic reticulum (Fig. 5, *arrowheads*). Furthermore, CLICK-III was also found to be enriched at the tips of thin processes that were most likely filopodia (Fig. 5, *arrows*); these structures have been proposed to constitute intermediate membrane protrusions that precede the formation of stable dendritic spines during synaptogenesis (38).

To better analyze in detail the potential mechanisms that might underlie the distinct localization of CLICK-III, we overexpressed CLICK-III in COS-7 cells. Ectopic expression of GFP-mCL3 in COS-7 cells confirmed that subcellular distribution of CLICK-III was indeed distinct from that of GFP or GFP-rCaMKIα. Unlike the diffuse distribution of GFP (Fig. 6*A*, *left panels*) or the largely cytoplasmic distribution GFP-rCaMKIα (Fig. 6*A*, *middle panels*), GFP-mCL3 localization overlapped with the perinuclear Golgi complex, as demonstrated by a high degree of spatial superimposition between GFP fluorescence of GFP-mCL3 and a Golgi-specific vital dye, BODIPY TR-ceramide (Fig. 6*A*, *right panels*, *arrows*). Such a co-localization was not detected between GFP-rCaMKIα, or GFP alone, and the BODIPY TR-ceramide stain (Fig. 6*A*, *upper panels*). In addition, a significant amount of GFP-mCL3 signals was seen at the plasma membranes (Fig. 6*A*, *right panels*, *arrowheads*). Consistent with such significant localization of GFP-mCL3 with the Golgi complex and the plasma membranes, a sizable pool of GFP-mCL3 protein was recovered in the membranes fraction (P), after 100,000 × *g* ultracentrifugation (Fig. 6, *B* and *C*). In contrast, GFP-rCaMKIα was predominantly present in the supernatants (S) and little in the membrane pellet fraction (P) (Fig. 6, *B* and *C*).

A Critical Role for a CAAX Motif in the Localization of CLICK-III to the Golgi Complex and Plasma Membranes—What might be the cause of such distinct subcellular localization between rCaMKIα and CLICK-III? Sequence search identified a putative *CAAX* membrane-anchoring motif in the very C-terminal end of mCLICK-III (Fig. 1 and Table I). We thus examined whether the *CAAX* box in mCLICK-III was necessary for its membrane localization. A single amino acid substitution at the putative prenylation site (GFP-mCL3C474S) completely abolished recruitment of mCL3 to the perinuclear Golgi (Fig. 7*A*, *left panels*, *arrows*) and plasma membranes (Fig. 7*A*,

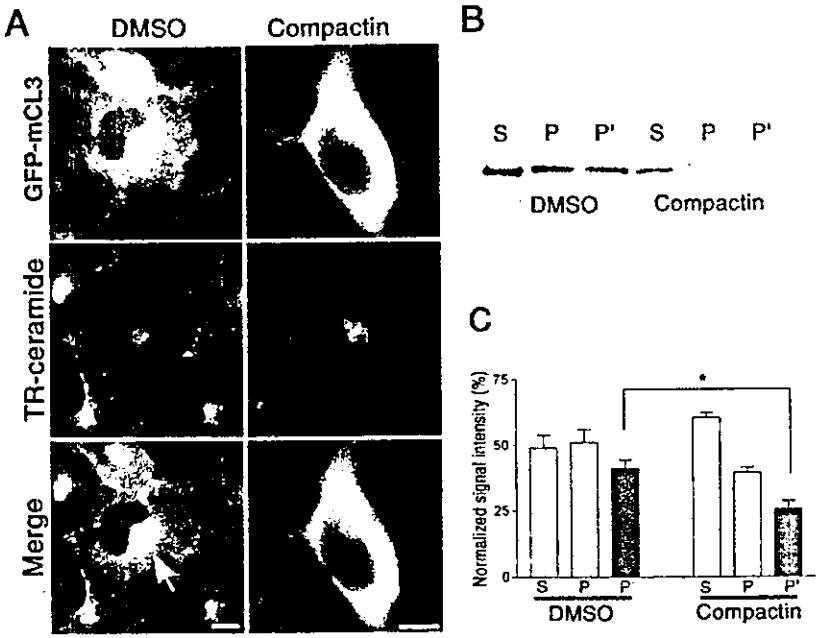

FIG. 8. **Compactin, an HMG-CoA reductase inhibitor, prevents GFP-mCL3 localization to the Golgi and plasma membranes.** *A*, COS-7 cells transfected with GFP-mCL3 were pretreated with vehicle alone (*DMSO*) or 40 μM compactin for 12 h, stained with BODIPY TR-ceramide, and examined under live conditions. The co-localization of GFP-mCL3 and BODIPY TR-ceramide (*arrow*) was abolished in compactin-treated cells. *Green*, GFP image; *red*, BODIPY TR-ceramide. *Bar*, 10 μm. *B*, COS-7 cells transfected with GFP-mCL3 were treated with 40 μM compactin for 16 h. The cytosolic fractions (*S*), the membrane fractions (*P*), the high salt-washed membrane fractions (*P'*) were collected and subjected to Western blotting using an anti-GFP antibody. *C*, quantification of signal intensities detected in *B*. The *bars* represent means ± S.E. (n = 5). * denotes $p < 0.05$.

left panels, *arrowheads*), and this mutant was now diffusely expressed in the cytoplasm (Fig. 7*A*, *middle panels*). Conversely, attachment of the *CAAX* box (CVLM) of the mCL3 to the C terminus of GFP (GFP-CLVM) was sufficient to confer perinuclear Golgi localization to GFP (Fig. 7*A*, *right panels*, *arrows*). We found, however, that GFP-CLVM did not appear to localize well to the plasma membranes, consistent with the notion that residues upstream of the *CAAX* motif may also play a role in the correct localization and the proper sorting to the plasma membranes (Fig. 7*A*, *right panels*) (22, 23). In accordance with these observations, biochemical fractionation experiments showed a significant reduction in the amount of membrane-bound GFP-mCL3C474S especially after high salt wash (P'), whereas GFP-CVLM still remained heavily associated with the membranes (Fig. 7, *B* and *C*). Together, these data suggested that the *CAAX* box of CLICK-III is necessary to localize CLICK-III to the Golgi membranes.

To confirm this point further, mCL3-overexpressing cells were pretreated with compactin, an HMG-CoA reductase inhibitor. As blockade of this rate-limiting step of cholesterol synthesis should also significantly reduce prenylation of the *CAAX* box cysteine (33), we expected that compactin treatment should mimic the effect of Cys-to-Ser mutation at position 474. Consistently, although vehicle (Me_2SO) treatment had no effect on localization of GFP-mCL3, which was strongly detected in association with Golgi and plasma membranes (Fig. 8*A*, *left panels*, *arrow*), an overnight compactin treatment dramatically abolished this membrane anchoring (Fig. 8*A*, *right panels*). Prevention of membrane recruitment of GFP-mCL3 and its retention to the soluble fractions by compactin treatment was also verified by using biochemical fractionation as well (Fig. 8, *B* and *C*).

Together, these experiments demonstrated that CLICK-III, a neuronally expressed CaMKI isoform, was able to be localized to the Golgi apparatus and plasma membranes, at least in part, via its C-terminal *CAAX* box in a prenylation-dependent manner.

DISCUSSION

CaMK represents a class of the multifunctional protein kinase family, with a particular significance for the physiology of excitable cells such as neurons or smooth muscles (1–10). A better understanding of the role of neuronal CaMKs has been of urgency because CaMK activity has been suggested to be crucial for linking neuronal activity with various types of neuronal plasticity (2–4, 8–11, 39–42). Recent experiments have further revealed that, in fact, various CaMK isoforms play a critical role in establishing distinct types of memory in mammals (9, 12, 43–46). So far, however, most analyses have focused on the role of CaMKIIα, β, and CaMKIV, because these are the most well characterized CaMKs widely expressed in forebrain neurons (35, 36). In contrast, studies concerning CaMKI have lagged behind, in part because the originally isolated CaMKIα has been expressed ubiquitously and little has been shown so far about its physiological role or substrates in neurons (13, 15, 17).

In this study, we have identified a neuronally enriched CaMKI isoform that has the potential to be membrane-anchored. This CaMKI isoform, CLICK-III/CaMKIγ, possessed an extended C-terminal domain distinct from known CaMKs. We found that CLICK-III had three particular characteristics that were noteworthy.

First, we confirmed that the activation of CLICK-III required not only Ca^{2+}/CaM but also a phosphorylation by other kinases, presumably by a CaMKK. Such strong CaMKK dependence for its enzymatic activation was qualitatively similar to what was reported previously for CaMKIα (27–29), indicating that the catalytic core of CLICK-III may resemble CaMKIα and may be regulated in a manner identical to CaMKIα. Thus, maximal activation of CLICK-III might only be triggered in close vicinity to an upstream kinase such as CaMKK.

Second, unlike CaMKIα, however, CLICK-III expression was strongly enriched in neurons. More interestingly, examination of its mRNA distribution, by *in situ* hybridization analyses, revealed a very strong expression in the CeA and the VMH. Such peculiar distribution stands out among all known CaMKs and indicates the possibility that CLICK-III may play a role in the proper function of these nuclei. The CeA has been shown to be a relay for most autonomic outputs and, furthermore, has been associated with the expression of the stimulus-specific state of fear (47). The VMH, on the other hand, has been linked

with control of the homeostasis of feeding and sexual behaviors (48, 49). Future studies are needed to determine whether some of these functions mediated through either CeA or VMH might indeed be controlled by the kinase activity of CLICK-III.

Third, our studies have clarified for the first time a mechanism by which CaMK may be anchored to the Golgi and plasma membranes. A *CAAX* motif that we identified in the unusually extended C-terminal end of CLICK-III played a critical role in determining the targeting of CLICK-III to the membrane compartments in a heterologous expression system. The high degree of sequence similarity of the *CAAX* motif of CLICK-III with that of Ras (Table I) and the disruption of membrane anchoring by either a point mutation at the putative prenylation site or by pretreatment with an HMG-CoA reductase inhibitor have suggested that prenylation of the *CAAX* box may constitute a mechanism through which CLICK-III may be actively sorted to the membranes. The prenyl moiety is derived from the mevalonate/cholesterol biosynthetic pathway. It is interesting to note that this pathway has been shown recently (50, 51) to affect various neuronal phenotypes. Furthermore, it is also notable that many neuronal signaling proteins (*e.g.* Ras, Rho, paralemmin, and PSD-95) have been modified by the addition of long fatty acid chains including prenylation and palmitoylation (52, 53). These post-translational modifications are suggested to play a critical role for precise membrane localization especially in highly polarized neuronal cells.

What could be the biological significance of such membrane targeting of a CaMK? In the case of Ras, *CAAX* box-dependent membrane anchoring was absolutely required to allow proper membrane recruitment of its downstream kinases, c-Raf and B-Raf (23). Similarly, *CAAX*-mediated localization of CLICK-III to the membranes might represent an advantageous mechanism to help tightly couple upstream signals to local downstream phosphorylation targets. In principle, a direct anchoring of CaMK activity to various membrane compartments is likely to facilitate the synaptic activity-induced local protein phosphorylation at or very close to the site of Ca^{2+} entry/mobilization. Whether such membrane-delimited excitation-phosphorylation coupling can indeed be triggered by electrical activity of the neurons, either postsynaptically or presynaptically, remains to be studied. Alternatively, or additionally, the presence of a CaMK in the Golgi apparatus might enable an efficient coupling of synaptic activity with intracellular trafficking of neuronal proteins. Experiments are underway to provide answers to these issues.

Acknowledgments—We are indebted to Drs. Masaaki Tsuda and Akiko Tabuchi (Toyama Medical and Pharmaceutical University), Dr. Hiroshi Tokumitsu (Kagawa Medical University), and Dr. Ryuichi Shigemoto (National Institute for Physiological Sciences) for comments during the course of the study. We are also grateful to Dr. Hirohide Takebayashi (National Institute for Physiological Sciences) for providing pIRES-S-Tag-EGFP and Dr. Hiroyuki Sakagami (Tohoku University) for sharing unpublished results. We thank Kimiko Nonomura for technical assistance and Tae Arai and Hiroko Nose for secretarial help.

REFERENCES

1. Berridge, M. J., Bootman, M. D., and Lipp, P. (1998) *Nature* **395,** 645–648
2. Bliss, T. V. P., and Collingridge, G. L. (1993) *Nature* **361,** 31–39
3. Schneggenburger, R., Sakaba, T., and Neher, E. (2002) *Trends Neurosci.* **25,** 206–212
4. Bito, H., Deisseroth, K., and Tsien, R. W. (1997) *Curr. Opin. Neurobiol.* **7,** 419–429
5. Bito, H. (1998) *Cell Calcium* **23,** 143–150
6. Soderling, T. R., and Stull, J. T. (2001) *Chem. Rev.* **101,** 2341–2352
7. Hook, S. S, and Means, A. R. (2001) *Annu. Rev. Pharmacol. Toxicol.* **41,** 471–505
8. Kennedy, M. B. (1994) *Annu. Rev. Biochem.* **63,** 571–600
9. Lisman, J., Schulman, H., and Cline, H. (2002) *Nat. Rev. Neurosci.* **3,** 175–190
10. Hudmon, A., and Schulman, H. (2002) *Annu. Rev. Biochem.* **71,** 473–510
11. Malinow, R., and Malenka, R. C. (2002) *Annu. Rev. Neurosci.* **25,** 103–126
12. Silva, A. J., Kogan, J. H., Frankland, P. W., and Kida, S. (1998) *Annu. Rev. Neurosci.* **21,** 127–148
13. Picciotto, M. R., Nastiuk, K. L., and Nairn, A. C. (1996) *Adv. Pharmacol.* **36,** 251–275
14. Fujisawa, H. (2001) *J. Biochem. (Tokyo)* **129,** 193–199
15. Yokokura, H., Terada, O., Naito, Y., Sugita, R., and Hidaka, H. (1997) *Adv. Second Messenger Phosphoprotein Res.* **31,** 151–157
16. Bito, H., Deisseroth, K., and Tsien, R. W. (1996) *Cell* **87,** 1203–1214
17. Picciotto, M. R., Zoli, M., Bertuzzi, G., and Nairn, A. C. (1995) *Synapse* **20,** 75–84
18. Verploegen, S., Lammers, J. W., Koenderman, L., and Coffer, P. J. (2000) *Blood* **96,** 3215–3223
19. Yokokura, H., Terada, O., Naito, Y., and Hidaka H. (1997) *Biochim. Biophys. Acta* **1338,** 8–12
20. Naito, Y., Watanabe, Y., Yokokura, H., Sugita, R., Nishino, M., and Hidaka, H. (1997) *J. Biol. Chem.* **272,** 32704–32708
21. Ueda, T., Sakagami, H., Abe, K., Oishi, I., Maruo, A., Kondo, H., Terashima, T., Ichihashi, M., Yamamura, H., and Minami, Y. (1999) *J. Neurochem.* **73,** 2119–2129
22. Choy, E., Chiu, V. K., Siletti, J., Feoktistov, M., Morimoto, T., Michaelson, D., Ivanov, I. E., and Philips, M. R. (1999) *Cell* **98,** 69–80
23. Zhang, F. L., and Casey, P. J. (1996) *Annu. Rev. Biochem.* **65,** 241–269
24. Tokumitsu, H., Brickey, D. A., Glod, J., Hidaka, H., Sikela, J., and Soderling, T. R. (1994) *J. Biol. Chem.* **269,** 28640–28647
25. Okuno, S., Kitani, T., and Fujisawa, H. (1994) *J. Biochem. (Tokyo)* **116,** 923–930
26. Tokumitsu, H., Enslen, H., and Soderling, T. R. (1995) *J. Biol. Chem.* **270,** 19320–19324
27. Haribabu, B., Hook, S. S., Selbert, M. A., Goldstein, E. G., Tomhave, E. D., Edelman, A. M., Snyderman, R., and Means, A. R. (1995) *EMBO J.* **14,** 3679–3686
28. Edelman, A. M., Mitchelhill, K. I., Selbert, M. A., Anderson, K. A., Hook, S. S., Stapleton, D., Goldstein, E. G., Means, A. R., and Kemp, B. E. (1996) *J. Biol. Chem.* **271,** 10806–10810
29. Matsushita, M., and Nairn, A. C. (1998) *J. Biol. Chem.* **273,** 21473–21481
30. Kitani, T., Okuno, S., and Fujisawa, H. (1997) *J. Biochem. (Tokyo)* **122,** 243–250
31. Anderson, K. A., Means, R. L., Huang, Q. H., Kemp, B. E., Goldstein, E. G., Selbert, M. A., Edelman, A. M., Fremeau, R. T., and Means, A. R. (1998) *J. Biol. Chem.* **273,** 31880–31889
32. Sheng, M., Thompson, M. A., and Greenberg, M. E. (1991) *Science* **252,** 1427–1430
33. Liao, J. K. (2002) *J. Clin. Invest.* **110,** 285–288
34. Oida, H., Namba, T., Sugimoto, Y., Ushikubi, F., Ohishi, H., Ichikawa, A., and Narumiya, S. (1997) *Br. J. Pharmacol.* **116,** 2828–2837
35. Erondu, N. E., and Kennedy, M. B. (1985) *J. Neurosci.* **5,** 3270–3277
36. Nakamura, Y., Okuno, S., Sato, F., and Fujisawa, H. (1995) *Neuroscience* **68,** 181–194
37. Sakagami, H., Umemiya, M., Saito, S., and Kondo, H. (2000) *Eur. J. Neurosci.* **12,** 89–99
38. Harris, K. M. (1999) *Curr. Opin. Neurobiol.* **9,** 343–348
39. Fukunaga, K., Muller, D., and Miyamoto, E. (1995) *J. Biol. Chem.* **270,** 6119–6124
40. Kasahara, J., Fukunaga, K., and Miyamoto, E. (2001) *J. Biol. Chem.* **276,** 24044–24050
41. Deisseroth, K., Bito, H., and Tsien, R. W. (1996) *Neuron* **16,** 89–101
42. Thiagarajan, T. C., Piedras-Renteria, E. S., and Tsien, R. W. (2002) *Neuron* **36,** 1103–1114
43. Ho, N., Liauw, J. A., Blaeser, F., Wei, F., Hanissian, S., Muglia, L. M., Wozniak, D. F., Nardi, A., Arvin, K. L., Holtzman, D. M., Linden, D. J., Zhuo, M., Muglia, L. J., and Chatila, T. A. (2000) *J. Neurosci.* **20,** 6459–6472
44. Ribar, T. J., Rodriguiz, R. M., Khiroug, L., Wetsel, W. C., Augustine, G. J., and Means, A. R. (2002) *J. Neurosci.* **20,** 1–5
45. Kang, H., Sun, L. D., Atkins, C. M., Soderling, T. R., Wilson, M. A., and Tonegawa, S. (2001) *Cell* **106,** 771–783
46. Wei, F., Qiu, C. S., Liauw, J., Robinson, D. A., Ho, N., Chatila, T., and Zhuo, M. (2002) *Nat. Neurosci.* **5,** 573–579
47. Davis, M., and Whalen, P. J. (2001) *Mol. Psychiatry* **6,** 13–34
48. Woods, S. C., and Stricker, E. M. (1999) *Fundamental Neuroscience* (Zigmond, M. J., Bloom, F. E., Landis, S. C., Roberts, J. L., and Squire, L. R., eds) pp. 1090–1101, Academic Press, New York
49. Flanagan-Cato, L. M., Calizo, L. H., and Daniels, D. (2001) *Horm. Behav.* **40,** 178–182
50. Matthies, H. Jr., Schulz, S., Hollt, V., and Krug, M. (1997) *Neuroscience* **79,** 341–346
51. Mauch, D. H., Nagler, K., Schumacher, S., Goritz, C., Muller, E. C., Otto, A., and Pfrieger, F. W. (2001) *Science* **294,** 1354–1357
52. El-Husseini, A. E.-D., and Bredt, D. S. (2002) *Nat. Rev. Neurosci.* **3,** 791–802
53. Kutzleb, C., Sanders, G., Yamamoto, R., Wang, X., Lichte, B., Petrasch-Parwez, E., and Kilimann, M. W. (1998) *J. Cell Biol.* **143,** 795–813

Article

ROCK and mDia1 antagonize in Rho-dependent Rac activation in Swiss 3T3 fibroblasts

Takahiro Tsuji,[1] Toshimasa Ishizaki,[1] Muneo Okamoto,[1] Chiharu Higashida,[1] Kazuhiro Kimura,[1] Tomoyuki Furuyashiki,[1] Yoshiki Arakawa,[1] Raymond B. Birge,[2] Tetsuya Nakamoto,[3] Hisamaru Hirai,[3] and Shuh Narumiya[1]

[1]Department of Pharmacology, Kyoto University Faculty of Medicine, Kyoto 606-8501, Japan
[2]Department of Biochemistry and Molecular Biology, University of Medicine and Dentistry of New Jersey, New Jersey Medical School, NJ 07214
[3]Department of Hematology and Oncology, Faculty of Medicine, University of Tokyo, Tokyo 113-8655, Japan

The small GTPase Rho acts on two effectors, ROCK and mDia1, and induces stress fibers and focal adhesions. However, how ROCK and mDia1 individually regulate signals and dynamics of these structures remains unknown. We stimulated serum-starved Swiss 3T3 fibroblasts with LPA and compared the effects of C3 exoenzyme, a Rho inhibitor, with those of Y-27632, a ROCK inhibitor. Y-27632 treatment suppressed LPA-induced formation of stress fibers and focal adhesions as did C3 exoenzyme but induced membrane ruffles and focal complexes, which were absent in the C3 exoenzyme-treated cells. This phenotype was suppressed by expression of N17Rac. Consistently, the amount of GTP-Rac increased significantly by Y-27632 in LPA-stimulated cells. Biochemically, Y-27632 suppressed tyrosine phosphorylation of paxillin and focal adhesion kinase and not that of Cas. Inhibition of Cas phosphorylation with PP1 or expression of a dominant negative Cas mutant inhibited Y-27632–induced membrane ruffle formation. Moreover, Crk-II mutants lacking in binding to either phosphorylated Cas or DOCK180 suppressed the Y-27632–induced membrane ruffle formation. Finally, expression of a dominant negative mDia1 mutant also inhibited the membrane ruffle formation by Y-27632. Thus, these results have revealed the Rho-dependent Rac activation signaling that is mediated by mDia1 through Cas phosphorylation and antagonized by the action of ROCK.

Introduction

Cells adopt different shapes in response to different stimuli. For example, interphase nonmotile Swiss 3T3 fibroblasts extend filopodia or lamellipodia or form stress fibers and focal adhesions in response to bradykinin, PDGF, and lysophosphatidic acid (LPA),* respectively, and these changes are mediated respectively by the Rho family small GTPases, Cdc42, Rac, and Rho (Hall, 1998). Migrating fibroblasts also exhibit lamellipodia, filopodia, and actin bundles with focal adhesions. However, in these cells those structures are observed in different places of a single cell. Filopodia and lamellipodia are seen in the leading edge of the cell, actin bundles similar to stress fibers are running from the front to the rear, and focal adhesions are at the tips of these bundles (Mitchison and Cramer, 1996; Horwitz and Parsons, 1999). It is also noteworthy that these structures change in space as the cell migrates. There is accumulating evidence that the Rho family small GTPases participate also in these shape changes of migrating cells (Allen et al., 1998; Nobes and Hall, 1999). However, how the activities of these GTPases are regulated spatiotemporally in migrating cells remains largely unknown.

The actions of the Rho GTPases are mediated by the respective groups of downstream effectors (Schmitz et al., 2000). Using the selective binding to the GTP-bound active form of Rho, several effectors of Rho were isolated (Narumiya, 1996). Among them, the ROCK–ROK–Rho kinase family of serine-threoine protein kinases has been found essential in Rho-induced formation of stress fibers and focal adhesions. Expression of a dominant negative form of this kinase or the addition of a specific inhibitor of this kinase Y-27632 inhibits stress fibers and focal adhesions induced by LPA or activated Rho in several cell lines (Ishizaki et al., 1997; Uehata et al.,

Address correspondence to Shuh Narumiya, Dept. of Pharmacology, Kyoto University Faculty of Medicine, Yoshida, Sakyo-ku, Kyoto 606-8501, Japan. Tel.: 81-75-753-4392. Fax: 81-75-753-4693. E-mail: snaru@mfour.med.kyoto-u.ac.jp

*Abbreviations used in this paper: FAK, focal adhesion kinase; GAP, GTPase-activating protein; GFP, green fluorescent protein; GST, glutathione *S*-transferase; LPA, lysophosphatidic acid; MT, microtubule.

Key words: Rho; mDia; Rac; membrane ruffles; Y-27632

The Journal of Cell Biology, Volume 157, Number 5, May 27, 2002 819–830
http://www.jcb.org/cgi/doi/10.1083/jcb.200112107

Supplemental Material can be found at:
http://www.jcb.org/cgi/content/full/jcb.200112107/DC1

1997). However, expression of a dominant active ROCK mutant alone leads to the formation of an aberrant form of centrally contracted actin bundles in the cell (Leung et al., 1996; Amano et al., 1997; Ishizaki et al., 1997), indicating that other Rho effector(s) cooperate to induce well-aligned stress fibers. We found recently that coexpression of an active mutant of another Rho effector, mDia1, corrected the alignment of actin bundles induced by active ROCK (Watanabe et al., 1999). Our subsequent study indicates that this mDia1 action is exerted through its action on microtubule (MT) alignment (Ishizaki et al., 2001). The structures of the actin cytoskeleton induced by ROCK and mDia1 reflect the pattern and location of focal adhesions induced by each of them. Dominant active ROCK mutants induce abnormally large adhesions not only in the cell periphery but also in the center of the cells. On the other hand, expression of active mDia1 mutants induces small adhesions at the tips of the cell. Theses results suggest that ROCK and mDia differently regulate shapes and locations of focal adhesions. However, how these two molecules affect signals and dynamics of focal adhesions remains unknown. There are several studies suggesting the regulation, by multiple Rho effector(s), of the processes involving the cell to substrate adhesion. For example, Nobes and Hall (1999) examined effects of C3 exoenzyme and Y-27632 on REF cells subjected to the in vitro wound healing assay and found that the C3 exoenzyme treatment abolished the cell migration, whereas Y-27632 stimulated it. Y-27632 was also reported not to block the G1 to S phase progression of the cell cycle in Swiss 3T3 cells (Ishizaki et al., 2000), which is sensitive to the C3 exoenzyme treatment (Yamamoto et al., 1993).

In this study, we compared the effects of C3 exoenzyme with those of Y-27632 first morphologically on rearrangement of actin cytoskeleton and focal adhesion and then biochemically on tyrosine phosphorylation of focal adhesion proteins. We also tested the effects of overexpression of several signaling molecules and inhibitors of Src and MT dynamics on the elicitation of the phenotype induced by ROCK inhibition. Our findings show that there is a dichotomy of the signaling from Rho, one being mediated by ROCK leading to tyrosine phosphorylation of focal adhesion kinase (FAK) and paxillin and the other mediated by mDia1 resulting in phosphorylation of Cas, and that the latter mDia1 pathway leads to activation of Rac, which is antagonistically regulated by the former ROCK pathway.

Results

Different effects of C3 exoenzyme and Y-27632 on LPA-induced actin reorganization and formation of focal adhesions in Swiss 3T3 cells

We stimulated serum-starved Swiss 3T3 fibroblasts with LPA and examined the effects of C3 exoenzyme that shuts off all of the Rho signals and those of Y-27632 that selectively inhibit ROCK-mediated pathway downstream of Rho. We first assessed their effects on actin cytoskeleton and focal adhesions by staining cells with phalloidin and antiphosphotyrosine antibody, respectively (Fig. 1 A). As originally shown by Ridley and Hall (1992), LPA addition to serum-starved 3T3 cells spread the cells and induced stress fibers and focal adhesions in a few minutes, and this change was completely inhibited by prior C3 exoenzyme treatment. The C3 exoenzyme-treated cells remained round with many beaded processes. On the other hand, the addition of Y-27632 did not affect the morphology of serum-starved cells, and when LPA was added to these cells they flattened and spread as seen in control cells. However, they did not develop actin stress fibers, but a thick rim of F-actin accumulation was seen in the cell periphery. Simultaneous staining with antiphosphotyrosine showed numerous small dot-like structures beneath this F-actin accumulation, which resembled Rac-induced focal complexes. Video microscopy revealed that LPA addition evoked robust membrane ruffles in the periphery of the Y-27632–treated cells (Fig. 1 B), suggesting that the thick actin rim detected by phalloidin staining represents membrane ruffles. We examined the specificity of this Y-27632 effect by two additional experiments. First, the addition of Y-27632 to the C3 exoenzyme-treated cells did not evoke LPA-induced cell spreading and membrane ruffles (Fig. S1 available at http://www.jcb.org/cgi/content/full/jcb.200112107/DC1). Second, the addition of PDGF could induce membrane ruffles in the C3 exoenzyme-treated cells (Fig. S2 available at http://www.jcb.org/cgi/content/full/jcb.200112107/DC1). These results indicate that the membrane ruffles seen in the Y-27632–treated cells occur in a Rho-dependent, ROCK-independent manner.

Rac is activated by a Rho-dependent, ROCK-independent signaling

Because membrane ruffles are usually induced by Rac activation, we suspected that Rac is activated under the above conditions and induces membrane ruffles in the Y-27632–treated cells. Therefore, we transfected Swiss 3T3 cells with dominant negative Rac (N17Rac) and examined the effect of its expression on the LPA-induced membrane ruffling in Y-27632–treated cells. As shown in Fig. 2 A, the cells expressing N17Rac showed no rim-like accumulation of F-actin in the periphery, and F-actin dispersed in the cytoplasm. Thin F-actin spikes were also seen around the cell periphery. These cells did not show dot-like accumulation of antiphosphotyrosine staining in the cell periphery either, and anti-phosphotyrosine staining accumulated in the cytoplasm as seen in C3 exoenzyme-treated cells. This phenotype was observed in 200 cells in a total of 235 cells observed in three independent experiments. These results suggest that activation of Rac occurred in the Y-27632–treated cells upon LPA addition and was responsible for membrane ruffle formation. To confirm this hypothesis biochemically, we performed the pull-down assay for GTP-Rac using a glutathione *S*-transferase (GST) fusion of the CRIB domain of Pak (Sander et al., 1998). As shown in Fig. 2 B, virtually no GTP-Rac was pulled down from lysates of any groups of serum-starved cells tested. A small but significant amount of GTP-Rac was precipitated from the lysates of the control cells stimulated with LPA. The precipitation of GTP-Rac was significantly enhanced in the Y-27632–treated cells stimulated with LPA and not in the C3 exoenzyme-treated cells. These results verified that Rac was activated in the Y-27632–treated cells upon LPA addition and suggest that this activation is induced by the Rho-dependent, ROCK-independent signaling.